Chapter 1

General Introduction, Scope and Contents of Present Work

This chapter presents the general introduction, scope, contents and aim of the present work. In this chapter, the basic theory related to dielectric and spectroscopic properties of ZnF_2-As_2O_3/WO_3-TeO_2 glasses are presented systematically.

General introduction Scope and Contents of present work

1.1 Introduction

Glass is an inorganic solid material that is usually clear or translucent with different colors. It is hard, brittle and stands up to the effects of wind, rain or Sun. In more precise terminology, glass is an amorphous solid completely lacking in long range, periodic atomic structure and exhibiting a region of glass transformation behavior. Any material, inorganic, organic or metallic, formed by any technique, which exhibits glass transformation behavior, is a glass.

The exceptionally rapid development of technological research in all fields of knowledge is accompanied by intense work by scientists and technologists on glass materials. These materials have potential applications as laser materials, IR domes, optical fibers, modulators, memory devices, photonic devices for communication and advanced computer applications and as semi conducting devices. Applications of these materials can also be found in nuclear waste management, optical fibers, solid electrolytes, electronic displays, biocompatible implants, dental posterior materials, high performance composites etc. In view of such vast and diversified applications, the investigation on the development and characterization of different glass materials has gained momentum in the recent years.

The literature survey on the formation of glass theories indicates that it was the Goldschmidt who proposed the theory of glass formation based on the

examination of various glass systems that glasses of the general formula R_nO_m form most easily when the ionic radius ratio of the cation, R, to the oxygen ion lies in the range 0.2 to 0.4. Since radius ratios in this range tend to produce cations surrounded by four oxygen ions in the form of tetrahedra, Goldschmidt believed that only melts containing tetrahedrally-coordinated cations form glasses during cooling. This contention was purely empirical, with no attempt to explain why tetrahedral coordination should be so favorable to glass formation. A few years later, Zachariasen extended the ideas of Goldschmidt and attempted to explain why certain coordination numbers might favor glass formation.

According to Zachariasen [1] there are only five oxide materials which form the glass by themselves viz., SiO_2, GeO_2, B_2O_3, As_2O_3 and P_2O_5; two more non-oxide compounds viz., As_2S_3 and BeF_2 are also added to this list recently [2]. Though, the glass materials do not possess the long-range periodicity but they retain short range order with AO_3 and AO_4 basic building blocks and follow certain rules proposed by Zachariasen. Basing on these rules, a continuous random network for a glass can be constructed as shown in Fig. 1.1.

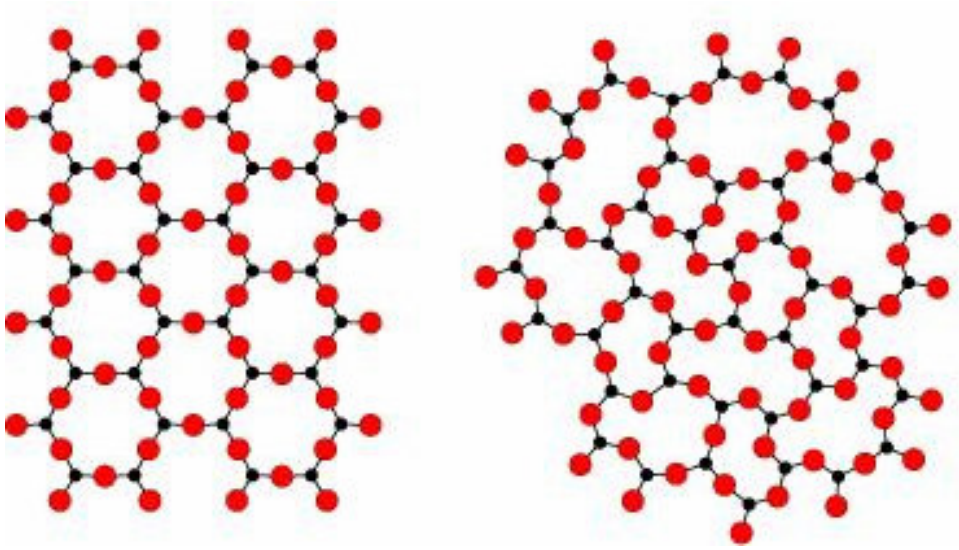

Crystalline A_2O_3 Glassy A_2O_3

Fig. 1.1 Two dimensional schematic of crystalline and non-crystalline (glass) materials.

As per these rules, the oxides of the type AO (CaO, BaO etc.), A_2O (Li_2O, Na_2O etc.) can not form glasses on their own and the rules are satisfied only for oxides of the type A_2O_3, AO_2 and A_2O_5 and for non-oxide compounds As_2S_3 and BeF_2. The cations such as A^+ (example Li^+, Na^+, K^+ etc.,) A^{2+} (example Ca^{2+}, Pb^{2+}, Cd^{2+} etc.,) other than A^{3+} and A^{4+} are known as network modifiers. Alkali oxides/fluorides, alkali earth oxides/fluorides, ZnO, PbO, CdO etc., are some of the basic examples of modifiers in glass network. These modifiers break-up the continuous network by introducing non-bridging oxygens (Fig.1.2).

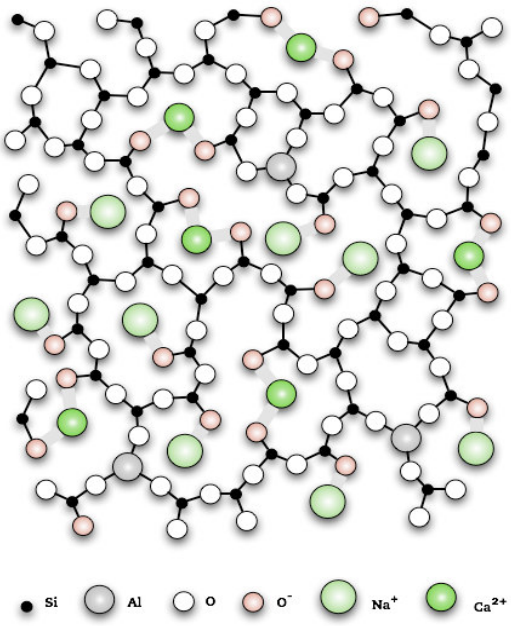

Fig. 1.2 Structure of a general glass with modifier oxides

A third group of oxides known as intermediate class of oxides also exist which by themselves not readily form glasses but do so when mixed with other oxides; such oxides are known as intermediate glass formers. The examples of this group include Sb_2O_3, Al_2O_3, Ga_2O_3, In_2O_3, TeO_2, WO_3, MoO_3, V_2O_5 etc.

The summary of the rules for glass formation proposed by Zachariasen is as follows:

a) A high proportion of glass network forming cations (Si, B, P, Ge, As, etc.,) is surrounded by oxygen tetrahedra or triangles.
b) The polyhedra, share should not more than one corner with each other
c) The number of corners of polyhedra is less than 6
d) Anions (O^{2-}, S^{2-}, F^-) should not be linked with more than two cations and do not form additional bonds with any other cations.
e) At least three corners of polyhedra must connect with the neighboring polyhedra.
f) The network modifiers participate in the glass network with the co-ordination number generally greater than 6.
g) Intermediate glass formers (do not form the glass on their own) but either reinforce network or loosen the network with co-ordination number 6 to 8 and may participate in the network with coordination number 3 or 4 in the presence of modifiers.

Excellent reviews and articles on the topology of the glass by Vogel [2], Elliott [3], Polk [4], Rao [5], Ingram [6] and Shelby [7] give useful information.

Glasses are traditionally formed by cooling the molten liquid. However, there are a number other non-conventional methods like chemical vapour deposition, solgel process techniques, etc. When a liquid is cooled from high temperature, crystallization may take place at the melting point T_m. If the crystallization takes place, there will be abrupt change in the volume/enthalpy at T_m. Continued cooling of the crystal will result in a further decrease in the volume/enthalpy due to the heat capacity of the crystal. If the liquid is cooled below the melting temperature without crystallization, a super cooled liquid is obtained. In this region, the structure of the liquid continues to rearrange as the temperature decreases, but there is no abrupt decrease in volume/enthalpy due to discontinuous structural rearrangement.

As the liquid is cooled further, the viscosity increases. This increase in viscosity eventually becomes so great that the atoms can no longer completely rearrange to the equilibrium liquid structure, during the time allowed by the experiment. The structure begins to lag behind that which would be present if sufficient time were allowed to reach equilibrium. The enthalpy begins to deviate from the equilibrium line, following a curve of gradually decreasing slope, until it eventually becomes determined by the heat capacity of the frozen

liquid, *i.e.,* the viscosity becomes so great that the structure of the liquid becomes fixed and is no longer temperature-dependent. The temperature region lying between the limits where the enthalpy is that of the equilibrium liquid and that of the frozen solid, is known as the glass transformation region. The frozen liquid is now a glass. The glass transition temperature lies in between these two temperatures, as such it is a fictious temperature and depends on the heating rate and previous thermal history of the sample.

This process of changes in volume/enthalpy with temperature as a super cooled liquid is cooled through the glass transition region is illustrated in Fig. 1.3.

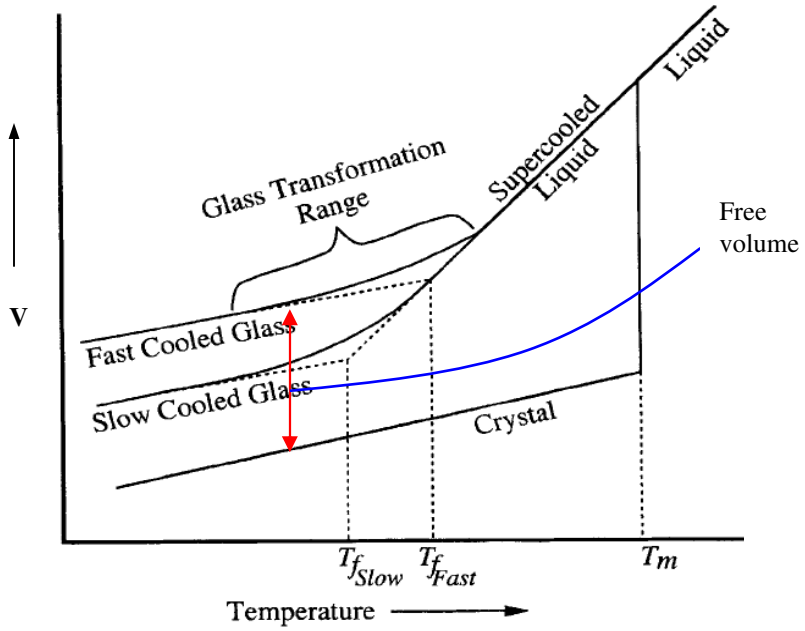

Fig. 1.3 Schematic illustration of the change in volume with temperature as super cooled liquid is cooled through the glass transition temperature T_g.

During the last few decades a variety of inorganic glasses have been developed with an attempt to achieve suitable electrical, mechanical and optical characteristics. These characteristics are associated with the improved physical properties such as electrical resistance, mechanical strength, glass transparency, IR transmission performance and their ability to accept more transition/rare earth metal ions for their use in solid-state devices. Work along these lines was carried out on a number of glasses giving valuable information [8-13]. Investigations on electrical properties such as dielectric properties of glasses help to have an idea over their insulating character. Investigations on the spectroscopic properties such as optical absorption, infrared spectra and electron spin resonance can be used as probes to throw some light on the structural aspects of these glasses. Studies on fluorescence spectra especially rare earth doped glasses will help to asses the suitability of the glasses for laser materials.

1.2 Scope of the present work

Among various glass systems tellurium oxide based glasses are the subject of intense current research because of their interesting electrical and optical properties. Compared with silicate and borate glasses, tellurite glasses have several superior physical properties such as high dielectric constant, high refractive index [14-16], large third order non-linear susceptibility [17], good chemical resistance and good infrared transmissivity [18]. Furthermore, these

glasses are transparent from the near ultraviolet to the middle infrared region. They are resistant to atmospheric moisture and are capable of accepting large concentrations of transitional metal ions and rare-earth ions [19]. In view of these qualities, tellurite based glasses were considered as potential candidates for laser hosts (since these provide a low phonon energy environment to minimize non-radiative loss [20]), in fiber optics, as nonlinear optical materials, as the best materials for optical components such as IR domes, optical filters, modulators, memories and laser windows [21].

The origin of these properties has been strongly correlated to the local order around tellurium atoms. The coordination geometry of Te atoms has been shown to be strongly dependent on the composition of the glasses and on the chemical nature of the glassy network modifier. For example, the addition of alkaline oxides in the TeO_2 matrix changes the coordination of Te from a TeO_4 trigonal bipyramid (tbp) group to a TeO_3 trigonal pyramid (tp) through intermediate polyhedra TeO_{3+1} (Fig. 1.4). The TeO_4 tbp group has two axial and two equatorial oxygen atoms, in which an electron pair occupies the third equatorial position of the sp^3d hybrid orbital. The presence of this electron pair plays a key role in the structure building and manifestation of nonlinear optical properties of tellurite glasses [22].

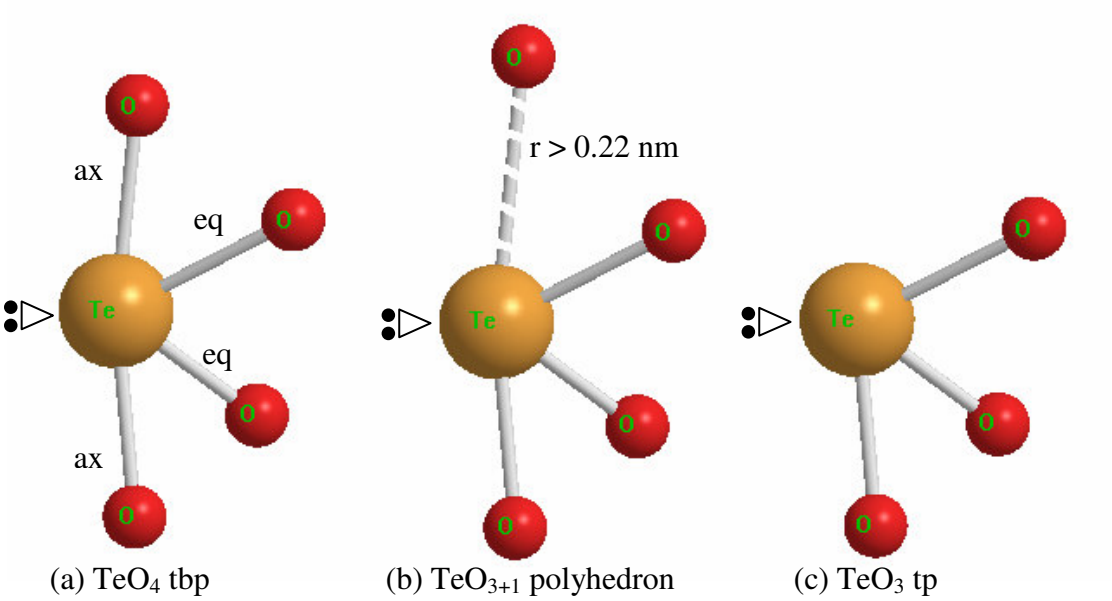

Fig. 1.4 Illustration of the coordination states of tellurium atom (a) TeO_4 trigonal bypyramid (tbp), (b) TeO_{3+1} polyhedron and (c) TeO_3 trigonal pyramid (tp)

Tellurium oxide is an incipient glass network former, hence the addition of strong network former like As_2O_3 to tellurium oxide glasses improves the glass forming ability and the optical transparency in the blue as well as in the IR regions [23]. As_2O_3 is the only strong network former besides GeO_2 that exhibit significant transmission potential farther into the infrared. This is illustrated by calculated wavelength of λ_o, the material dispersion crossover point which is 1.3 μm for P_2O_5, B_2O_3 and SiO_2, 1.7 μm for GeO_2 and 1.9 μm for As_2O_3 [24, 25]. The addition of As_2O_3 is expected to affect the infrared transmission of TeO_2 glasses to a less extent, since the frequencies of some of the fundamental modes of vibration of As_2O_3 structural groups lay in the region of vibrations of TeO_4 structural groups [25]. In view of this, it is also predicted that AsO_3 groups form a single arsenic–tellurium–oxygen framework with the TeO_4 structural units and may strengthen the glass network. Addition of the modifier like ZnF_2 to TeO_2–As_2O_3 glass matrix is expected to lower the viscosity and to decrease the liquidus temperature to a substantial extent and makes the glass more moisture resistant [26].

Similarly, the addition of WO_3 to tellurite glasses makes them suitable for optoelectronic devices since they exhibit photochromism and electrochromism properties and influences profoundly the luminescence characteristics of rare earth ions in tellurite glasses, since these ions exist in

different valence states viz., W^{6+}, W^{5+} and also in W^{4+} and offer varying environment for luminescent ions in the glass network.

Though considerable studies on electrical properties along with optical properties [27–29] of some TeO_2 based glasses are available in literature, majority of these studies are devoted to binary tellurite glasses and further they are mainly concentrated on dc conductivity studies [30–33]. Much devoted studies on electrical properties, especially on dielectric relaxation and ac conductivity of ZnF_2–As_2O_3–TeO_2 glass system doped with transition metal ions like V_2O_5 and NiO are very rare; knowledge on these properties is highly helpful for estimating the influence of these oxides on the insulating strength of tellurite glasses and may also pave way for the analysis of the structure of this glass system to some extent if these studies are coupled with the other studies like optical absorption, ESR, infrared, Raman and luminescence spectra.

The first row transition metal ions are very interesting ions to probe in the glass network because their outer d-electron orbital functions have rather broad radial distributions and their responses to surrounding actions are very sensitive; as a result these ions influence the physical properties of the glasses to a substantial extent.

Three series of elements are formed by filling the 3d, 4d and 5d shells of electrons. Together these comprise the d–block elements. They are often called ‘transition elements’ because their position in the periodic table is between s-

block and p-block elements. Their properties are transitional between the highly reactive metallic elements of the s-block, which typically form ionic compounds, and the elements of p–block, which are largely covalent. In s-and p-blocks, electrons are added to the outer shell of the atom where as in d-block they are added to the penultimate shell. Typically transition elements have an incompletely filled d level.

In the d-block elements, the penultimate shell of electrons is expanding. Thus they have many physical and chemical properties in common and hence all the transition elements are metals. They are therefore good conductors of electricity and yet have a metallic luster and are hard, strong and ductile. They also form alloys with other metals.

Table 1.1 Oxidation states of transition metal elements.

Element	Sc	Ti	V	Cr	Mn	Fe	Co	Ni	Cu	Zn
Electronic structure	d^1s^2	d^2s^2	d^3s^2	~~d^4s^2~~ d^5s^1	d^5s^2	d^6s^2	d^7s^2	d^8s^2	~~d^9s^2~~ $d^{10}s^1$	$d^{10}s^2$
Oxidation numbers					7					
				6	6	6				
			5	5	5	5	5			
		4	4	4	4	4	4	4		
	3	3	3	3	3	3	3	3	3	
		2	2	2	2	2	2	2	2	2
		1	1	1	1	1	1	1	1	

One of the most striking features of the transition metal elements is that they usually exist in several oxidation states (Table 1.1). Furthermore, the oxidation states change in units of one, e.g. V^{4+} and V^{5+}, Ni^{2+} and Ni^{3+}, W^{4+} and W^{5+}.

Among these, Mn can have an oxidation state of +7 due to the hypothetical loss of 7 electrons ($4s^2\ 3d^5$) - after this nuclear charge binds electrons more strongly. The number of unpaired electron decreases steadily on either side of Mn. The pattern shown below:

Among the first five transition metal elements, the correlation between the electronic structures and minimum and maximum oxidation states in simple compounds is complete. In the highest oxidation states of these first five elements, all of the s and d electrons are being used for bonding. Thus the properties depend only on size and valency, and consequently show some similarities with elements of the main groups in similar oxidation states. If the d^5 configuration is exceeded, i.e. in the last five elements, the tendency for all the d electrons to participate in the bonding decreases.

The covalent radii of the elements decrease from left to right across a row in the transition series, until near the end when the size increases slightly. On passing from left to right, extra protons are placed in the nucleus and extra orbital electrons are added. The orbital electrons shield the nuclear charge incompletely (d electrons shield less efficiently than p electrons, which in turn

shield less effectively than s electrons). Because of this poor screening by d electrons, the nuclear charge attracts all of the electrons more strongly: hence a contraction in size occurs.

Recently, much attention has been paid to research in inorganic glasses doped with transition metal ions because of their technological importance in the development of tunable solid state lasers, new luminescence materials, solar energy converters and fiber optic communication devices. In view of these, it is felt worthwhile to have some understanding over the dielectric and spectroscopic properties of ZnF_2–As_2O_3–TeO_2 glasses doped with two transition metal (viz., vanadium and nickel) ions. The studies on dielectric properties and the dependence of these properties on the composition, structure and on various external factors such as humidity, radiation effect, mechanical action etc., pave the way for estimating the insulating character. Whereas the investigations on spectroscopic (viz., optical absorption, electron spin resonance, infrared and photoluminescence spectra) properties give the information on environment and the oxidation states of the transition metal ions in the glass network and also help to assess the suitability of these glasses for practical applications.

As mentioned above the tellurite glasses mixed with WO_3 offers highly suitable environment for hosting the rare earth ions to give out high luminescence output with low phonon losses. In view of this, a part of the

thesis is devoted to investigate the fluorescence characteristics of three interested rare earth ions viz., Nd^{3+}, Sm^{3+} and Eu^{3+} ions in ZnF_2–WO_3–TeO_2 glass system.

A preliminary description of the above-mentioned properties along with their relation to some of the investigations (similar to those of present work) on ZnF_2–As_2O_3/WO_3–TeO_2 glasses is given below:

1.2.1 *Physical parameters*

Some physical parameters useful for characterization ZnF_2–As_2O_3/WO_3–TeO_2 glasses doped with transition metal oxides and rare earth oxides are estimated from the measured value of density (d) and the average molecular weight $\overline{M}$, using the following equations [34–37]:

The transition metal ion concentration (N_i) could be obtained from:

$$N_i = \frac{N_A \, M(\text{mol}\%) \, d}{\overline{M}} \tag{1.1}$$

From the N_i values obtained, the polaron radius (r_p) and inter–ionic distance (r_i) of transition metal ions could be evaluated:

$$\text{Inter–ionic distance (Å)}, \; r_i = \left[\frac{1}{N_i}\right]^{1/3} \tag{1.2}$$

$$\text{Polaron radius (Å)}, \; r_p = \frac{1}{2}\left[\frac{\pi}{6N_i}\right]^{1/3} \tag{1.3}$$

The field strength (F_i) of transition metal ion in the glass matrix is described through the oxidation number (z) and the ionic radii (r_p) of the transition metal ions by:

$$\text{Field strength (cm}^{-2}\text{)},\ F_i = \frac{z}{r_p^2} \qquad (1.4)$$

1.2.2 *Dielectric properties*

When an insulating glass (a dielectric) like ZnF_2–As_2O_3–TeO_3 glass is placed in external electric field two types of polarizations – the electronic and the ionic – are expected to develop in the glass. If the dielectric contains permanent dipoles, they experience a torque in an applied field that tends to orient them in the field direction. Consequently, an orientational (or dipolar) polarization can arise. These three polarizations are due to charges locally bound in atoms, molecules or in the structures of solids. Additionally to all these, generally there exist charge carriers that can migrate for some distance through the dielectric. Such charge carriers during their motion may be trapped in the material or on interfaces (because they cannot be freely discharged or replaced at the electrodes); due to these causes, space charges and a microscopic field distortion result. Such a distortion appears as an increase in the capacitance of the sample and may be indistinguishable from a real rise of the dielectric constant. Thus a fourth polarization, called the space charge

polarization comes into play. The total polarization is sum of these four polarizations (assuming that they act independently) [38].

When the dielectric is placed in alternating fields, these polarizations are set up and the dielectric constant is a consequence of them; also a temporal phase shift is found to occur between the applied field and the resulting polarization and a loss current component appears, giving rise to the dielectric loss of the sample [39].

The complex dielectric constant, according to Debye for a material having permanent dipoles characterized by single relaxation time τ, given by:

$$\varepsilon^* = \varepsilon_\infty + \frac{\varepsilon_s - \varepsilon_\infty}{1 + i\omega\tau} \tag{1.5}$$

Where, ε_s is the static dielectric constant and ε_∞ is the dielectric constant value of the material corresponding to its electronic and atomic polarization. Separating this equation into its real and imaginary parts, one obtains:

$$\varepsilon'(\omega) = \frac{\varepsilon_s - \varepsilon_\infty}{1 + \omega^2\tau^2} \tag{1.6}$$

and

$$\varepsilon''(\omega) = \frac{(\varepsilon_s - \varepsilon_\infty)\omega\tau}{1 + \omega^2\tau^2} \tag{1.7}$$

The dielectric loss of the material (generally expressed by tan δ) is given by the expression:

$$\varepsilon''(\omega) = \frac{(\varepsilon_s - \varepsilon_\infty)\omega\tau}{1 + \omega^2\tau^2} \tag{1.8}$$

If the conductivity (σ_{ac}) of the sample is also taken into account, it can be shown that

$$\tan \delta = \frac{4\pi\sigma}{\omega \varepsilon'(\omega)} + \frac{(\varepsilon_s - \varepsilon_\infty)\omega\tau}{\varepsilon_s + \varepsilon_\infty \omega^2 \tau^2} \qquad (1.9)$$

By plotting log (tanδ) as a function of log(ω), information regarding ac conductivity as well as the behaviour of the dipoles present if any can be obtained.

1.2.3 *Optical absorption*

Optical radiation interacts with materials in a variety of ways depending upon the material and the wavelength of the optical radiation-giving rise to the optical spectra, which could be either emission or absorption spectra in solids, normally it is the absorption spectra, which is observed. This is nothing but the variation of the radiation intensity as a function of wavelength. Study of the absorption spectra of transition metal ions embedded in solids had been extensively used to obtain information about the local symmetry in which the ion sits in its valence state, its site preference and determination of the degree of covalency of the metal-ligand bond. When a transition metal ion is embedded in a glass it need not have a centre of symmetry. This leads to mixing of d– and p– orbitals of the ion and, therefore, an electronic transition involves some charge transfer from a d-orbital to a p-orbital leading to weak absorption bands. If an ion is at the centre of symmetry, such a mixing does not

occur but during the inevitable molecular vibrations make an ion spend part of the time away from the equilibrium position, which enables mixing of d– and p– orbitals and allow such transitions.

Most of the physical properties of the transition metal complexes are studied with the help of crystal field, ligand field and molecular orbital theories. The ligand field theory explains the optical levels by energy splitting of the states of the central ion in the field of the surrounding atoms. The theory of this splitting under the influence of fields produced by various symmetries has been worked out recently [40–42]. The principal symmetry of the transition metal complexes is usually an octahedral one while in a few cases, tetrahedral, square planar and lower symmetries occur. In a complex the site symmetry of anions is always degraded from the extremely high spherical one to a lower symmetry. Two types of symmetries, known as octahedral (designated by O_h) and tetrahedral (designated by T_d) are important. The corresponding molecular structures having these symmetries are shown diagrammatically in Fig. 1.5.

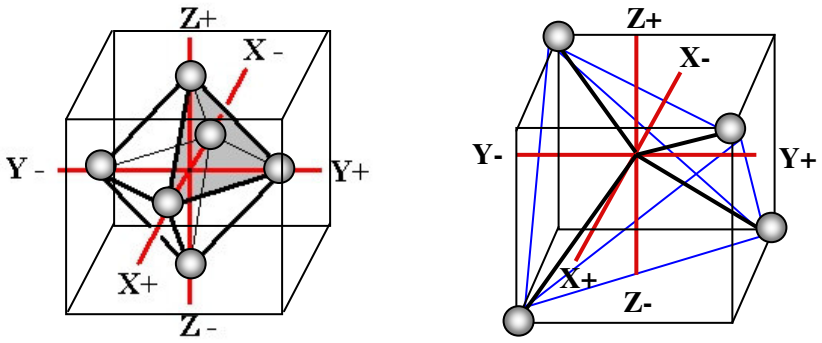

Fig. 1.5 (a) Regular Octahedron point group (O_h)
(b) Regular Tetrahedron point group (T_d)

A free d-electron has five-fold degeneracy with all the five d-orbitals, namely d_{xy}, d_{yz}, d_{zx}, $d_x^2{-}_y^2$ and d_z^2 possessing the same energy (Fig.1.6a). In a weak field approach, one tries to understand the effect of crystal fields on the free ion terms. In a weak field approach, one tries to understand the effect of crystal fields on the free ion terms (Fig. 1.6 b, c, d).

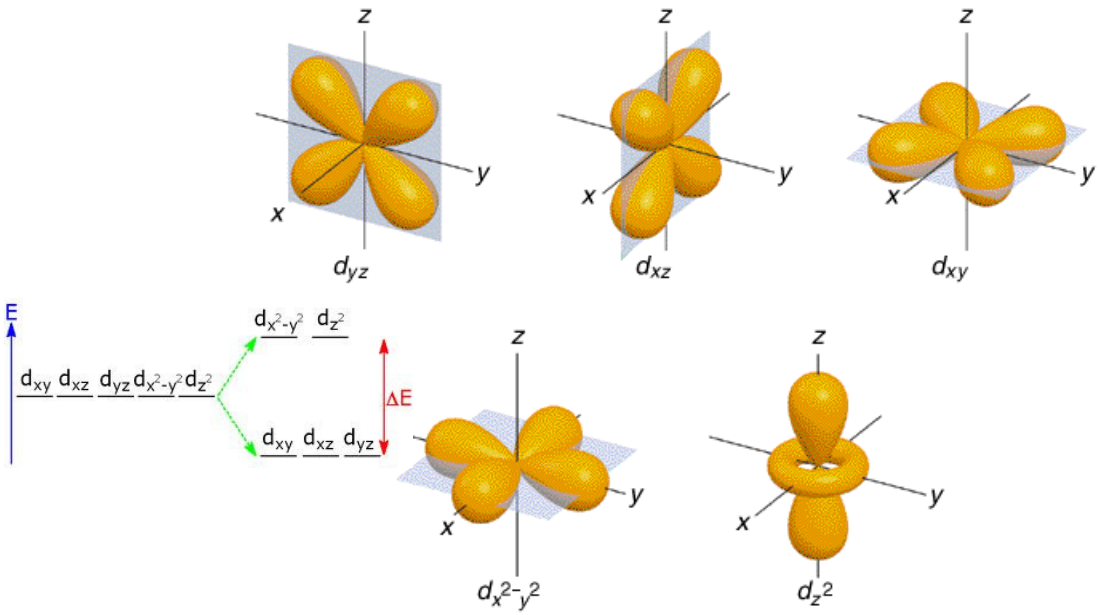

Fig. 1.6 (a) Five d orbitals of T_{2g} orbitals and e_g orbitals.

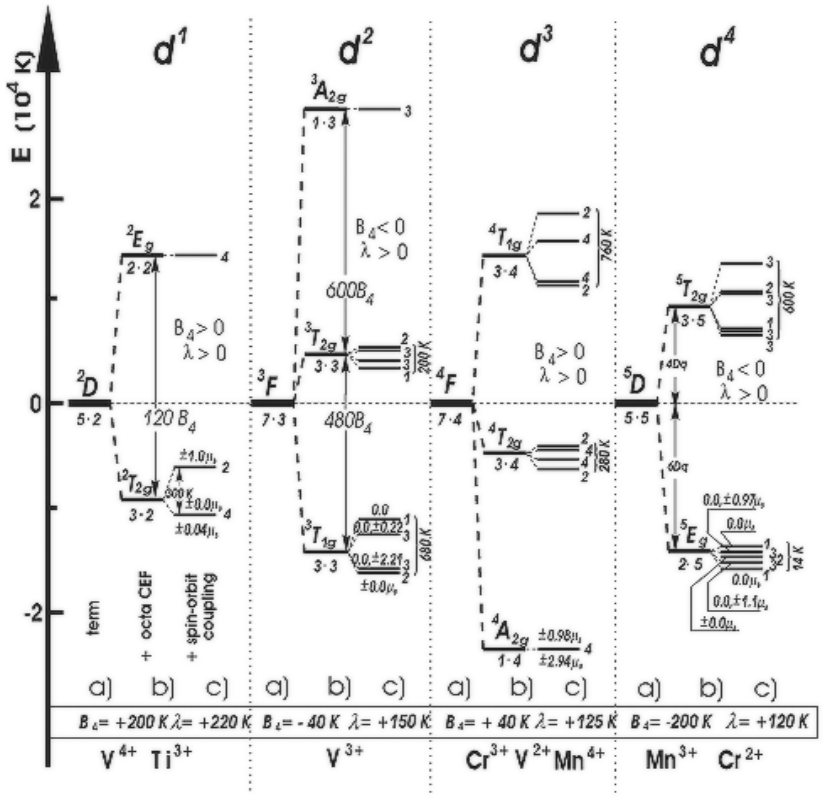

Fig. 1.6 (b) Detailed spectral information on various transition metal (from d^1 to d^4) ions.

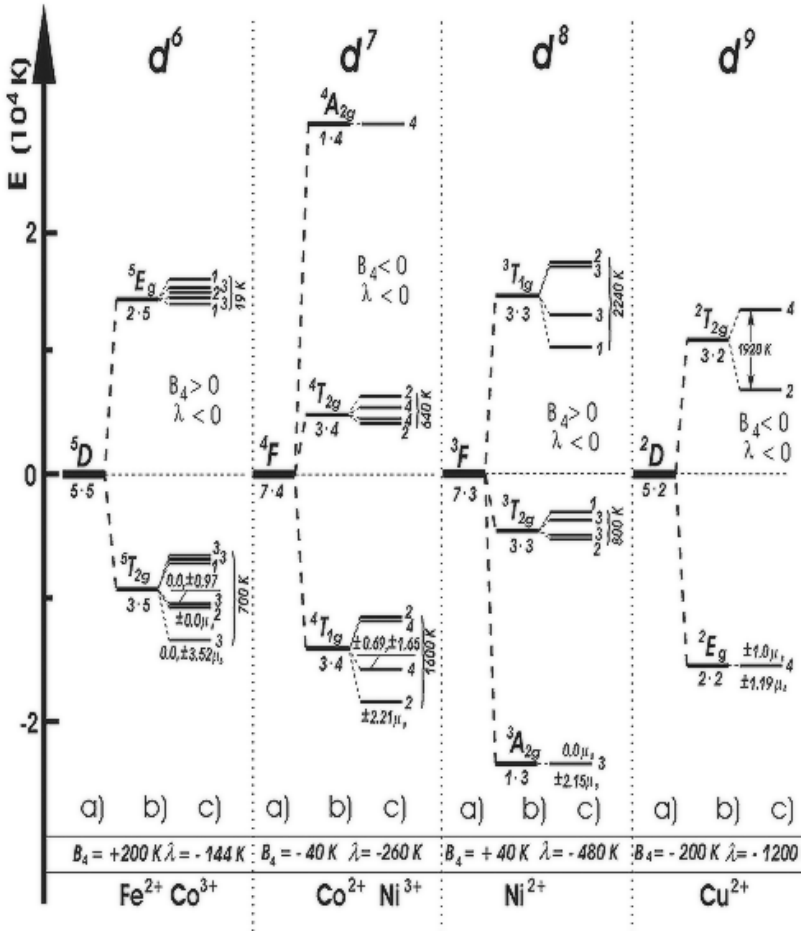

Fig. 1.6 (c) Detailed spectral information on various transition metal (from d^6 to d^9) ions.

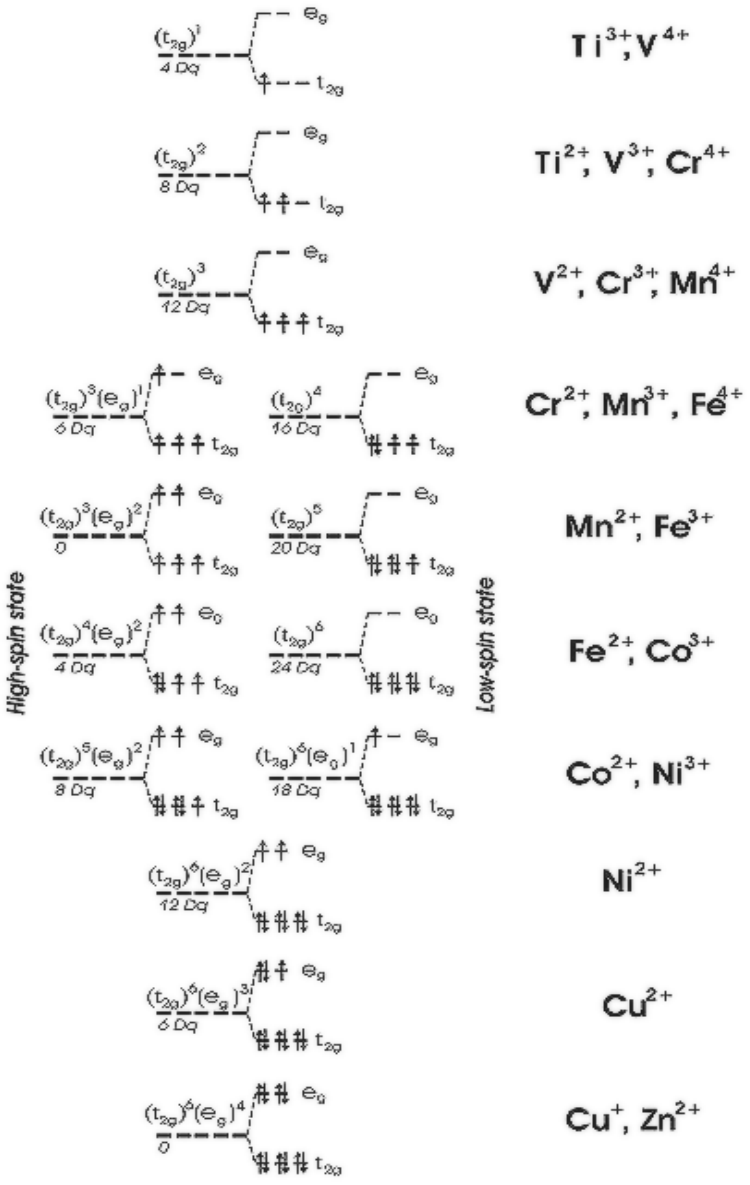

Fig. 1.6 (d) Energy spectra of transition metal ions.

For d case, the application of the group theory results in the splitting of ^2D state into e_g and t_{2g} representations in octahedral crystal field. The crystal field potential acting on the ion is given by

$$V_{oct} = D(x^4+y^4+z^4-(3/5)r^4) \quad (1.10)$$

where $D = (Ze/4a^5)$. This potential has to be applied on the wave functions which transform as t_{2g} whereas $d_{x^2-y^2}$ and d_{z^2} transform as e_g, and

$$\langle t_{2g}/V_{oct}/t_{2g}\rangle = -4D_q \quad (1.11)$$

$$\langle e_g/V_{oct}/e_g\rangle = 6D_q \quad (1.12)$$

Thus, the separation to D_q between t_{2g} and e_g levels is a measure of the crystal field. The centre of gravity of the levels is preserved after application of the crystal field potential.

In tetrahedral (T_d) symmetry, the nature of the splitting is the same but ordering of the levels is inverted as shown in Fig. 1.7. If the symmetry is lower than octahedral, say tetragonal or orthorhombic, then these levels will split into levels of lesser degeneracy. The above discussion is valid for single electron d orbitals. Similar procedure is adopted for multi electron system where the terms will be split into various irreducible representations.

In the case of strong octahedral crystal fields, the single electron t_{2g} and e_g functions become the basis. The various configurations many electron systems are obtained by filling the t_{2g} shell first and then the e_g shell. Thus for example, the d^2 ion has t_{2g}^2, $t_{2g}^1.e_g^1$ and e_g^2 configurations with energies - $8D_q$, $2D_q$ and $12D_q$, respectively.

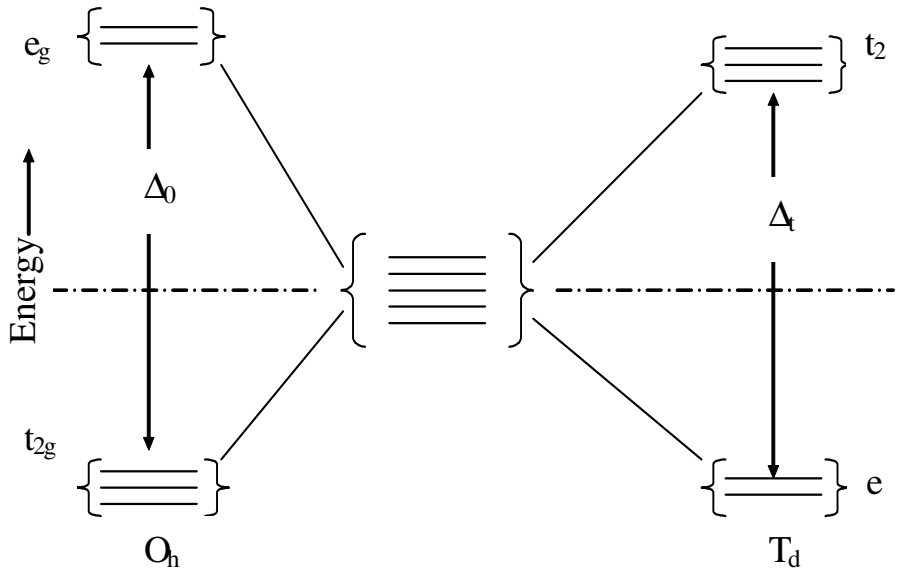

Fig. 1.7 Diagram showing relative energy of e_g and T_{2g} orbitals resulting the splitting of d orbitals by octahedral environments.

The electrostatic energy values for different states have been calculated by Tanabe and Sugano [43] and Griffith [44] and they have presented these energy values in the form of matrices. For convenient interpretation of the observed optical spectra, Tanabe and Sugano have drawn energy level diagrams between E/B and D_q/B for various d^n configurations known as Tanabe-Sugano diagrams. Here, E corresponds to the energy level of a d^n system and B is the Racah inter−electronic repulsion parameter. These diagrams are mainly used in crystal field spectroscopy to evaluate the crystal field parameter D_q and parameters B and C. From these diagrams, it is possible to obtain a quantitative measure of the ease of spin pairing. These diagrams also help in assigning the transitions correctly.

1.2.4 *Electron spin resonance*

Electron spin resonance (ESR) has been developed as an extremely sensitive and important spectroscopy technique, which is widely used to study systems having unpaired electrons. In condensed matter physics, ESR is used as a powerful technique to study the lowest energy levels, hence, the electronic state of the unpaired electrons of paramagnetic species in solids. This technique provides information on understanding of the symmetry of the surroundings of the paramagnetic ion and the nature of its bonding to the nearest diamagnetic neighbors. Following are a few examples of systems containing unpaired electrons.

1. Atoms having odd number of electrons, e.g., atomic hydrogen and lithium atom.
2. Molecules with odd number of electrons such as NO, and triplet state molecules like oxygen molecule.
3. Ions having partially filled inner electronic shells, e.g., iron, rare earth ions etc.
4. Defects produced in a solid by irradiation.
5. Free radicals, e.g., CH_3 and diphenyl−picrylhydrazyl.
6. Conduction electrons in metals, semiconductors and dilute alloys etc.

When a system having non-zero angular momentum and magnetic moment is placed in an external magnetic field, each degenerate electronic

level splits into a number of levels depending upon the value of angular momentum (Zeeman splitting). The ESR technique, basically, is the observation of the transitions induced by an electromagnetic radiation of appropriate polarization and energy (frequency) between these Zeeman levels. The energy separation of these levels is typically of the order of 1 cm^{-1} (microwave frequency range) in atomic and molecular systems. Thus, a microwave spectrometer is normally required to observe ESR.

An electron possesses spin and associated with it is the spin angular momentum "S" in units of ħ. An electron in a system like an atom or ion will also have, in general, an angular momentum "L" in units of ħ. The total angular momentum "J" is then given by

$$\vec{J} = \vec{L} + \vec{S}. \tag{1.13}$$

Associated with the total angular momentum J, the magnetic dipole moment μ given by

$$\vec{\mu} = -g\beta\vec{J} \tag{1.14}$$

where

$$g = 1 + \frac{J(J+1) + S(S+1) - L(L+1)}{2J(J+1)} \tag{1.15}$$

which is known as the Lande splitting factor for free ion and

$$\beta = \frac{e\hbar}{2mc} = 9.274096 \text{ X } 10^{-27} \text{ erg/gauss} \tag{1.16}$$

which is known as the Bohr magneton. When a magnetic dipole is placed in a uniform magnetic field B, it precesses about the direction of B with the Larmor angular frequency ω_L which is given by [45]

$$\omega_L = \gamma B \tag{1.17}$$

where $\gamma = g \beta / \hbar$ is known as gyromagnetic ratio. Thus, the resonance condition will be satisfied only when the frequency of the incident radiation is given by

$$h\nu = g \beta B. \tag{1.18}$$

When an electromagnetic radiation of a frequency ν is applied to the sample, the resonant absorption of the energy by the unpaired electrons in the sample takes place whenever the resonance condition is satisfied.

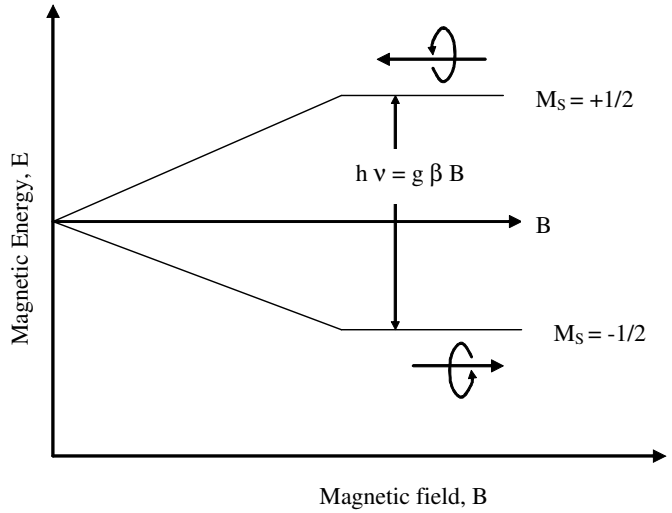

Fig. 1.8 Zeeman energy for a single unpaired electron as function of magnetic field B. A magnetic dipole aligned parallel to B has lower energy while a magnetic dipole aligned antiparallel to B has higher energy.

The energy level of an electron with total angular momentum J has a degeneracy of (2J + 1). The application of an external magnetic field removes this degeneracy and the energy level splits into (2J + 1) levels. When angular momentum L is zero then J becomes equal to S. The transitions between these levels are governed by the selection rules $\Delta M_s = \pm 1$, where M_s is the spin magnetic quantum number. An unpaired electron with $S = \pm 1/2$, when placed in a uniform magnetic field B, will have two energy levels, as shown in Fig. 1.8, if g is constant. The energies of these levels are

$$E_{\pm 1/2} = \pm(1/2) g \beta B, \tag{1.19}$$

and the energy difference between the two levels for a given value of B is

$$\Delta E = g \beta B \tag{1.20}$$

The above equation shows that the energy difference between the two levels increases linearly with B in the ESR technique. The magnetic dipole transitions between the levels are induced between the two levels in the presence of a uniform magnetic field B and an alternating magnetic field polarized perpendicular to B by an incident radiation of frequency ν if the quantum condition (1.18) and $\Delta M_s = \pm 1$ are satisfied. This will give rise to only one absorption line. When the orbital angular momentum is not zero then the degenerate energy level will split into (2J+1) levels and the conditions for the transitions by absorption of energy is given by Eq. (1.18) and $\Delta M_J = \pm 1$. Such a situation will give rise to multiple absorption lines. The resonance

condition (1.18) can be satisfied either by changing the magnetic field or the frequency of the radiation incident on the magnetic dipole. Practically, it is more convenient to vary the uniform magnetic field rather than the frequency of the incident radiation since the frequency variation of a microwave source is possible within a very small range only.

Thus, from an ESR spectrum recording one can get information about the resonance field at a fixed frequency of the electromagnetic radiation, hence, the 'g' value, the shape, amplitude and width of the absorption line. The 'g' value may be modified by the crystal field surrounding the free ion from the value of the "free ion value". All of these parameters, when interpreted properly and in conjunction with the appropriate theoretical ideas, provide valuable information on the system studied. In addition, one may vary certain other external parameters like temperature, composition etc., which would possibly change ESR parameters leading to additional information on the system under study. A vast discussion on ESR technique and its applications is available in a number of pioneering books written by many authors [46–50].

a) General Spin- Hamiltonian

In ESR spectroscopy, the transitions can be observed between the energy levels of ground state. In order to get the eigen values and eigen functions, we need to solve the Schrödinger's time- dependent equation applied on Hamiltonian operator. For a Hamiltonian consisting of more than

one term, the easier way to solve the equation is by perturbation theory. Here the eigen value is found by taking the strongest interaction and then the next interaction will be treated as a perturbation of the levels obtained in the first case. This procedure is repeated until the weakest interaction is included. This method suffers with a draw back that various interactions should differ from one another by at least one or two orders of magnitude. Incidentally, this condition is satisfied in EPR spectroscopy.

The Hamiltonian, which describes various interactions of unpaired electrons with the static magnetic field and that of the surrounding environment, can be formalized in terms of spin operators. The coefficient of spin operators is called spin–Hamiltonian parameters.

The concept of Hamiltonian was originally developed by Pryce [51] and Abragam and Pryce [52] to interpret the observed resonance of ions in the first transition series. The concept was subsequently extended by Elliott and Stevens [53] to interpret the paramagnetic behavior observed for the rare earth ions. The terms in the general Hamiltonian for an ion in a crystalline environment can be written as [54].

$$H = H_E + H_{LS} + H_{SI} + H_Q + H_V + H_{SH} + H_{lH} \qquad (1.21)$$

Where the symbols indicate the type of interaction to which Hamiltonian applies and have the following meaning.

i. H_E is a composite term expressing the total energy of electrons, the columbic attractions of the electrons and the nuclei and the repulsion among the electrons

ii. $$H_E = \sum_i \left[\frac{P_i^2}{2m} - \frac{Ze^2}{r_i} \right] + \sum_{ij} \frac{e^2}{r_{ij}} \qquad (1.22)$$

Where P_i is the momentum of i^{th} electron, r_i is the distance of the electron from the nucleus, r_{ij} is the distance between the i^{th} electron and j^{th} electron and Ze is the nuclear charge.

These terms are summed over all the electrons and yield the unperturbed electronic levels before considering the interaction between spin and orbital angular momenta. The separations will be of the order 10^5 cm^{-1}.

iii. H_{LS} represents the spin-orbit coupling and may be written in the form.

$$H_{LS} = \sum \lambda_{ij} \bullet l_i \bullet s \qquad (1.23)$$

Where l is the orbital angular momentum of the individual electron, 's' is the spin angular momentum of the individual electron and λ_{ij} is the spin – orbit coupling constant. This can be written in a simple form as

$$H_{LS} = \lambda \ \mathrm{L} \bullet S \qquad (1.24)$$

Where, L and S are the total orbital angular momentum and the spin angular momentum of free ion respectively. The magnitude of this interaction lies in the range 10^2 to 10^3 cm^{-1}.

iv. H_{SI} describes the magnetic interaction between each electron and the nucleus

$$H_{SI} = \sum a_i \bullet \mathbf{J}_i \bullet \mathbf{I}_i \qquad (1.25)$$

Where $\mathbf{J}_i$ is the total angular momentum of the i^{th} electron and $\mathbf{I}_i$ is the nuclear spin. The magnitude of this interaction will be of the order of 10^{-2} cm^{-1}.

v. H_Q represents the nuclear quadrupole interactions, which are even smaller than H_{SI} (~ 10^{-4} cm^{-1}) and may be neglected. For nuclei with spin $\mathbf{I} > ½$, these interactions shift the hyperfine levels by a small amount.

$$H_Q = \sum \mathbf{I}_i \bullet \mathbf{Q}_i \bullet \mathbf{I}_i \qquad (1.26)$$

vi. H_v represents the effect of crystal field, which can be written as

$$H_v = \sum e_i \ \mathbf{V}(r_i) \qquad (1.27)$$

Where $\mathbf{V}(r_i)$ is the electrostatic potential at the ion with which each electron interacts.

In an external magnetic field B, the terms H_{SH} and H_{IH} must be added to represent the interaction of the angular momentum of electrons and nuclei respectively with the magnetic field.

$$H_{SH} = \beta \ (\mathbf{L} + g_e \ \mathbf{S}) \cdot \mathbf{B} \qquad (1.28)$$

$$H_{IH} = \mathbf{h} / 2\pi \sum_i - \gamma_i \cdot \mathbf{I}_i \cdot \mathbf{B} \qquad (1.29)$$

Where γ_i is the gyrometric ratio of the i^{th} nucleus and the latter terms (about

10^{-4} cm^{-1}) may be neglected expect in considering second order effects in the nuclear hyperfine interaction.

b) Line shapes

The most commonly observed shape functions in EPR spectroscopy are Lorentzian and Gaussian, described by the functions given below.

$$\mathbf{I} = \frac{I_0}{T_2^2 (B - B_r)^2 + 1} \qquad (1.30)$$

$$\mathbf{I} = I_0 \exp [-b (B-B_r)^2 T_2^2] \qquad (1.31)$$

Where I_0 is the intensity of the absorption at its centre, B_r is the resonant field at the line centre. The constants T_2^2 and b are related to the half width of each of the two types of curves.

The Lorentzian shape arises due to harmonically bound electron. If the harmonic motion of the electron is interrupted by some process, then the distribution of frequencies follow the Eq. (1.31) for an EPR spectrum, the interruption will be in the form of exchange. Since all the electrons are equivalent, their interchanging between two molecules is quite possible if the molecules are close enough to each other. If this exchange is so rapid to affect the phase coherence of the spins, Lorentzian shape results.

On the other hand, Gaussian shape results from the paramagnetic ion separated from each other by molecules, which are having no unpaired electrons but possessing magnetic nuclei. Each unpaired electron will

experience a local static magnetic field which will be dominated by how the nuclear spins are arranged in the near by host molecules. The observed EPR spectra will be a superposition of shapes from all the spins with their local fields. Since the local fields will be randomly distributed, the total line shape results in a Gaussian line shape according to Eq. (1.30). The characteristic Lorentzian and Gaussian line shape are shown in the Fig. 1.9.

c) Line Width and Intensities

Generally the EPR signals are recorded as the first derivative of the absorption curve and hence the area under the EPR signal can be calculated by numerical double integration method. In this method, the EPR spectrum is divided in to 'n' small intervals having length'd'. The height hr of the EPR signal corresponding to the centre of r^{th} interval is noted and the area under the curve can be calculated from the equation

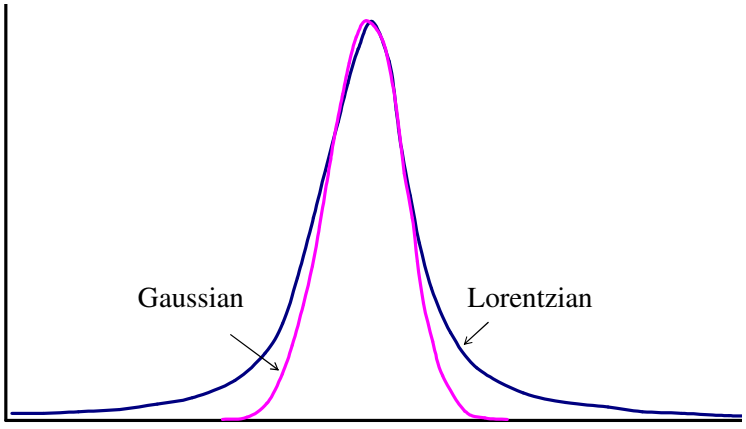

Fig. 1.9 The characteristic Lorentzian and Gaussian line shapes.

$$\mathbf{A} \quad = \quad \mathbf{1/2} \;\; d^{\,2} \sum_{r=1}^{n} \left(n - 2r + 1\right) \mathrm{h_r} \qquad (1.32)$$

Fig. 1.10 shows the method of finding the area under the first derivative absorption curve by numerical double integration method. The accuracy of this method depends on the number of intervals and complexity of the spectrum. Using about 8 to 10 intervals per peak, the error in calculating the area will likely be within 2 to 3% in Gaussian curves. For Lorentzian curves, the error may be greater due to the presence of long tails.

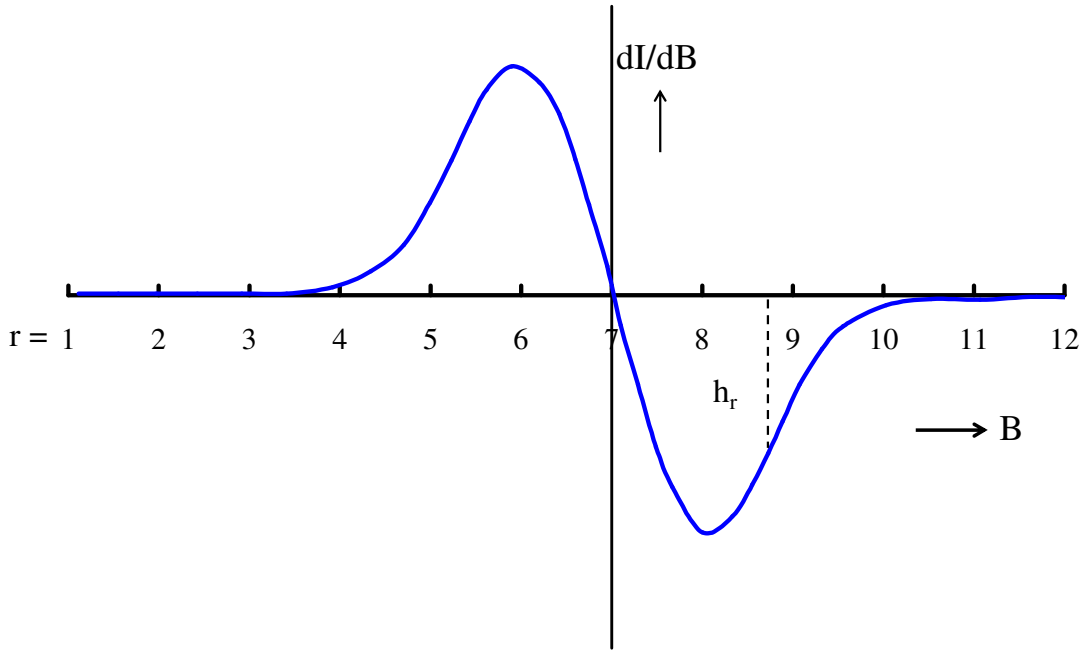

Fig. 1.10 The method of finding the area under the first derivative absorption curve by numerical double integration method.

For ESR signals, the line widths are measured from the maximum and minimum line positions at the first derivative curve. The ESR lines always have a finite width due to electrons interacting magnetically with the

environment of the sample. Hence, from the line width and the rate of build up or decay of the line intensity, one can obtain information about spin environment.

The intensity of ESR signals depends on various factors: (1) concentration of the paramagnetic ion, (2) the microwave frequency, (3) the power of microwaves, (4) the transition probability and (5) the temperature.

1.2.5 *Magnetic susceptibility*

Many compounds of the transition elements are paramagnetic, because they contain partially filled electron shells. If the magnetic moment is measured, the number of unpaired electrons can be calculated. The magnetochemistry of the transition elements shows whether the d electrons are paired. This is of great importance in distinguishing between high spin and low spin octahedral complexes. Thus, the magnetic moment μ of a transition metal ion can give important information about the number of unpaired electrons present in the ion and the orbital that are occupied, and sometimes indicates the structure of the molecule or complex.

The magnetic susceptibility measurements were under taken with a view to evaluate magnetic moments of the transition metal ions there by knowing whether these ions are in the tetrahedral or octahedral positions. The susceptibility of the nickel ion doped ZnF_2–As_2O_3–TeO_2 glass powders were

measured at room temperature using Guoy's balance. From the paramagnetic susceptibility χ, the magnetic moment μ is determined using the relation,

$$\chi = N\mu^2/3KT. \quad (1.33)$$

Here, N is the concentration of the paramagnetic ions, K is the Boltzmann constant and T is the temperature in Kelvin scale.

1.2.6 *Infrared spectra*

Infrared absorption spectra of glasses can provide significant and valuable information on the arrangement of atoms, nature of chemical bonding between them, the changes in the atomic configurations caused by increase or decrease of concentration of glass−forming systems and in general, facilitate the probing of the short-and intermediate range in glass networks.

In addition, the investigation of infrared spectra (IR) of glasses enables the assignment of characteristic frequencies to molecular groups in the glasses and hence correlation of IR absorption bands with different units of vitreous structure. In the case of arsenate tellurite glasses, the basic glass contains AsO_3, TeO_4, TeO_3 structural units in the glass network and when a cation such as Zn is added, it may reside interstitially. Such information about the changes in the basic glass structure that take place upon the addition of a cation can also be studied from the IR spectra.

The vibrations of structural units in glasses are independent [55–57], unlike the vibrations of complex ions in a glass matrix which are dependent of

the vibrations of other groups. In probing the structural units and changes that take place in the network with composition of a ternary glass, infrared spectroscopy lends itself as an effective tool, because the technique is sensitive to short-range ordering and local interactions.

The assignment of the important IR bands observed in ZnF_2–As_2O_3/WO_3–TeO_2 glasses of the present work is in general made by comparison of the data with the bands observed in literature, even though some bands attributions have their support from the theory. However, it is possible to provide quantitative justification from the theoretical calculation in the literature [56] for some of the vibrational frequencies assigned to arsenate, tellurite oxide and other transitional ion groups like VO_4, VO_6, NiO_4, NiO_6 etc.

When the characteristic group frequencies arise from the vibrations of pure stretching character or of pure bending nature the wavenumber– $\bar{\nu}$ is to given by the equation

$$\bar{\nu} = \frac{1}{2\pi c}\left(\frac{K}{\mu}\right)^{1/2} \tag{1.34}$$

where c is the velocity of light, m is the reduced mass of the diatomic or triatomic group, K is the stretching or bending force constant. For certain diatomic and triatomic groups, the force constant was evaluated using various empirical formulae available in the literature [56, 57].

1.2.7 *Raman spectra*

Among variety of spectroscopic methods, Raman spectroscopy provides information about molecular symmetry of relatively small molecules and functional groups in large and complex molecules. Raman spectroscopy became a useful technique with the introduction of lasers as a convenient monochromatic light source. It has become widely available only after the introduction of holographic filters to reject the light scattered without frequency change. In this method, the sample is illuminated with monochromatic light (a laser) and the light scattered by the material is analyzed by a conventional optical microscope coupled to a Raman spectrometer or a very sophisticated filter. Most of the scattered light has the same frequency as the laser, but a very tiny amount experiences a frequency shift, which is characteristic of the chemical bonds or molecules present in the material. This inelastic scattering of light is called the Raman effect. The analysis of the scattered frequencies (*Raman spectroscopy*) gives information on the material chemical composition, state, aggregation, and even factors like stress, orientation etc. The difference in energy between incident photon and the scattered photon occurs as a result of the coupling between incident radiation and the quantized states of target material. The incident photon can lose (stokes) or gain (anti-stokes) energy by a vibrational quantum of the target molecule. The energy increase or decrease from the excitation is related to the

vibrational energy spacing from the ground electronic state of the molecule and therefore the wavenumber of the Stokes and anti-Stokes lines are a direct measure of the vibrational energies of the molecule. A schematic Raman spectrum may appear as in Fig. 1.11.

In Raman spectrum, the Stokes and anti-Stokes lines are equally displaced from the Rayleigh line. This occurs because in either case one vibrational quantum of energy is gained or lost. Also, note that the anti-Stokes line is much less intense than the Stokes line. This occurs because only molecules that are vibrationally excited prior to irradiation can give rise to the anti-Stokes line. Hence, in Raman spectroscopy, only the more intense Stokes line is normally measured. For a vibrational motion to be IR active, the dipole moment of the molecule must change. For a transition to be Raman active there must be a change in polarizability of the molecule with the vibrational motion. Thus, Raman spectroscopy complements IR spectroscopy. For example, homonuclear diatomic molecules do not have an infrared absorption spectrum, because they have no dipole moment, but do have a Raman spectrum, because stretching and contraction of the bond changes the interactions between electrons and nuclei, thereby changing the molecular polarizability. For highly symmetric polyatomic molecules possessing a center of inversion (such as benzene) it is observed that bands that are active in the IR spectrum are not active in the Raman spectrum (and vice-versa). In molecules with little or no

symmetry, modes are likely to be active in both infrared and Raman spectroscopy.

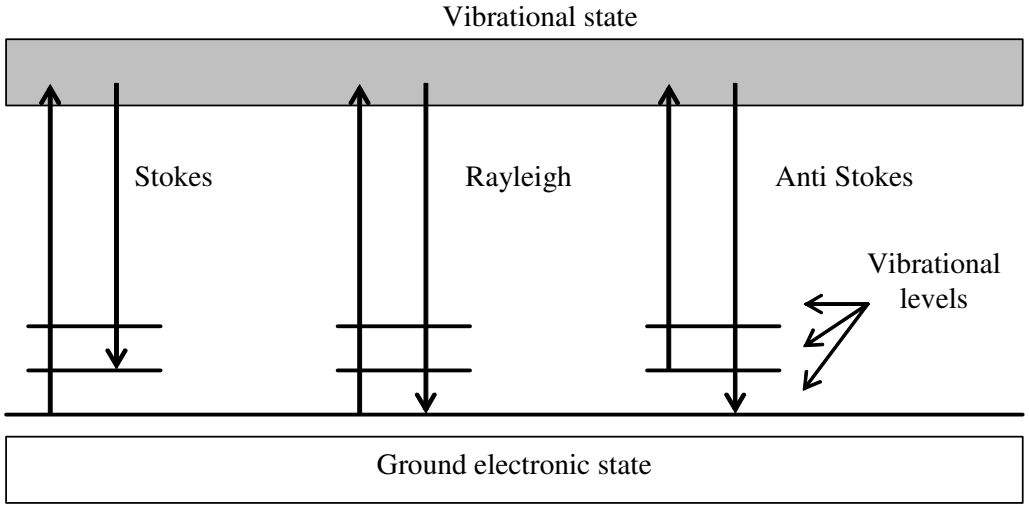

Fig. 1.11 A schematic representation of Raman spectrum

In the present study, the Raman spectroscopy has been used for identifying various structural units like WO_3, WO_4, TeO_4 structural groups in the ZnF_2–WO_3–TeO_2 glass matrix and the changes in the concentration of these structural units with the varying concentration of WO_3. In certain cases, it could also be possible to identify whether the tungsten ion occupy either tetrahedral or octahedral positions in the glass network.

1.2.8 *Rare earth ions and optical properties*

In the periodic Table, elements from lanthanum (Z=57) to lutetium (Z=71) are known as lanthanides. These are f-block elements with $4f^{n}\,5s^{2}\,5p^{6}$ as the outer most electronic configuration of the trivalent states of these elements. As the 4f sub shell of these ions is filled there is shrinkage in the volume of these ions and this is known as lanthanide contraction. This contraction is due to imperfect shielding from the nuclear charge of one f electron followed by another electron. All the rare-earths exist in trivalent state and some occasionally in divalent and tetravalent states. These rare- earth ions are associated with the f-f and f-d transitions. In the present study three rare earth ions viz, Nd^{3+}, Sm^{3+} and Eu^{3+} are incorporated into the ZnF_2–WO_3–TeO_2 glasses.

The fact that the shielding of outermost electrons of these rare earth ions, makes them to serve as active centers in the solid state laser hosts like the present ZnF_2–WO_3–TeO_2 glasses. These ions exhibit sharp absorption and luminescence transitions. Since, these 4f ions are weakly perturbed by the surrounding ligands [58]. The spectral intensities have been carried out with the help of Judd-Ofelt theory [59]. The spectral intensities are often expressed in terms of oscillator strength (f). Experimentally, this can be calculated from the following expression:

$$f_{exp} = 2.303\ (mc^2/N_A)\,\pi\, e^2 \int \varepsilon(\nu) d\nu \qquad (1.35)$$

Where N_A = Avagadro`s number, c is the velocity of light and ε (ν) = molar absorption coefficient, which is evaluated from Beer`s law:

$$\varepsilon(\nu) = \frac{1}{LC}\log(I_0/I)) \tag{1.36}$$

with *C* being the rare earth ion concentration (mol %), *L* the optical path length (thickness) and $\log(I_0/I)$ the optical density. After substituting the constants, Eq. (1.35) reduces to:

$$f_{exp} = 4.319^{*}\ 10^{-9}\int \varepsilon(\nu)d\nu \tag{1.37}$$

According to the conventional Judd–Ofelt (JO) theory [59, 60], the calculated OS of the electric dipole transition between two states can be expressed as follows:

$$f_{cal} = \frac{8\pi^2 mc\nu\chi}{3h(2J+1)}\sum_{\lambda=2,4,6}\Omega_\lambda\left\langle f^N[\gamma,S,L]J\left\|U^\lambda\right\|f^N[\gamma',S',L']J'\right\rangle^2 \tag{1.38}$$

where *m* is the electron mass, *c* the speed of light, *h* the Planck constant, $\chi = \frac{(n^2+2)^2}{9n}$ the local field correction, *n* is the refractive index, and the bra- and ket-vectors $\left\langle f^N[\gamma,S,L]J\right|$, $\left|f^N[\gamma',S',L']J'\right\rangle$ stand for the initial and final states, respectively, with all necessary sets of quantum numbers in square brackets. $\left\|U^\lambda\right\|$ are the reduced matrix elements of the unit tensor operators calculated between the states involved into a considered transition [34].

Admitting that the f-f transitions are mainly due to electric dipoles [35], the following selection rules are used:

$$\Delta l = +1;\ \Delta S = 0,\ \Delta L < 2,\ \Delta J < 2 \qquad (1.39)$$

where l = 3 for the lanthanides. Using Judd–Ofelt parameters (Ω_λ), the radiative properties of the fluorescence levels could be determined. The spontaneous emission probability for an electric dipole transition is obtained from [61];

$$A_{JJ'} = \frac{64\pi^4 e^2 \nu^3}{3h(2J+1)} \frac{n\left(n^2+2\right)^2}{9} \sum_{\lambda=2,4,6} \Omega_\lambda \left\langle f^N[\gamma,S,L]J \left\| U^\lambda \right\| f^N[\gamma',S',L']J' \right\rangle^2 \qquad (1.40)$$

where *e* is the charge of electron, and all other quantities are the same as in Eq. (1.38). The values of $\|U^\lambda\|^2$ taken from the literature for various absorption transitions of Nd^{3+}, Sm^{3+} and Eu^{3+} are presented in Tables 1.2 (a–c)] [34, 62, 63].

Table 1.2 (a) Reduced matrix elements for different absorption levels of Nd^{3+} ions.

(Ground term: $^4I_{9/2}$)

Transition $\Psi_J \rightarrow \Psi_{J'}$	Energy (cm^{-1})	$\|\| U^2 \|\|^2$	$\|\| U^4 \|\|^2$	$\|\| U^6 \|\|^2$
$^4I_{11/2}$	2007	0.0194	0.1073	1.1652
$^4I_{13/2}$	4005	0.0001	0.0136	0.4557
$^4I_{15/2}$	6080	0.0000	0.0001	0.0452
$^4F_{3/2}$	11527	0.0000	0.2293	0.0549
$^4F_{5/2}$	12573	0.0010	0.2371	0.3970
$^2H_{9/2}$	12738	0.0092	0.0080	0.1154
$^4F_{7/2}$	13460	0.0000	0.0027	0.2352
$^4S_{3/2}$	13565	0.0010	0.0422	0.4245
$^4F_{9/2}$	14854	0.0009	0.0092	0.0417
$^2H_{11/2}$	16026	0.0001	0.0027	0.0104
$^4G_{5/2}$ (HST)	17167	0.8979	0.4093	0.0359
$^2G_{7/2}$	17333	0.0757	0.1848	0.0314
$^2K_{13/2}$	19018	0.0068	0.0002	0.0312
$^4G_{7/2}$	19103	0.0550	0.1570	0.0553
$^4G_{9/2}$	19544	0.0046	0.0608	0.0406
$^2K_{15/2}$	21016	0.0000	0.0052	0.0143
$^2G_{9/2}$	21171	0.0010	0.0148	0.0139
$(^2D, ^2P)_{3/2}$	21266	0.0000	0.0188	0.0002
$^4G_{11/2}$	21563	0.0000	0.0053	0.0080
$^2P_{1/2}$	23140	0.0000	0.0367	0.0000
$^2D_{5/2}$	23865	0.0000	0.0002	0.0021
$(^2P, ^2D)_{3/2}$	26260	0.0000	0.0014	0.0008
$^4D_{3/2}$	28312	0.0000	0.1960	0.0170
$^4D_{5/2}$	28477	0.0001	0.0567	0.0275
$^2I_{11/2}$	28624	0.0049	0.0146	0.0034
$^4D_{1/2}$	28894	0.0000	0.2584	0.0000
$^2L_{15/2}$	29260	0.0000	0.0248	0.0097
$^2I_{13/2}$	29966	0.0001	0.0013	0.0017
$^4D_{7/2}$	30554	0.0000	0.0037	0.0080
$^2L_{17/2}$	30747	0.0000	0.0010	0.0012
$^2H_{9/2}$	32567	0.0001	0.0085	0.0000
$^2D_{3/2}$	33481	0.0000	0.0112	0.0012
$^2H_{11/2}$	33913	0.0001	0.0001	0.0002
$^2D_{5/2}$	34474	0.0007	0.0006	0.0034
$^2F_{5/2}$	38504	0.0021	0.0033	0.0000
$^2F_{7/2}$	39926	0.0000	0.0004	0.0007
$^2G_{9/2}$	47696	0.0000	0.0015	0.0001
$^2G_{7/2}$	48586	0.0004	0.0024	0.0002

Table 1.2 (b) Reduced matrix elements for different absorption levels of **Sm^{3+}** ions.

(Ground term: $^6H_{5/2}$)

Transition $\Psi_J \rightarrow \Psi_{J'}$	Energy (cm^{-1})	$\| U^2 \|^2$	$\| U^4 \|^2$	$\| U^6 \|^2$
$^6H_{13/2}$	5014	0.0000	0.0010	0.0660
$^6H_{15/2}$	……..	0.0000	0.0000	0.0040
$^6F_{1/2}$	……	0.1938	0.0000	0.0000
$^6F_{3/2}$	……..	0.1444	0.1365	0.0000
$^6F_{5/2}$	7033	0.0330	0.2844	0.0000
$^6F_{7/2}$	7900	0.0020	0.1430	0.4300
$^6F_{9/2}$	9075	0.0000	0.0210	0.3416
$^6F_{11/2}$	10460	0.0000	0.0006	0.0516
$^4G_{5/2}$	17860	0.0000	0.0100	0.0000
$^4M_{15/2}$	…….	0.0000	0.0000	0.0320
$^4I_{11/2}$	20977	0.0000	0.0000	0.0111
$^4I_{13/2}$	21562	0.0000	0.0030	0.0237
$^6P_{5/2}$	23784	0.0000	0.0244	0.0000

Table 1.2 (c) Reduced matrix elements for different absorption levels of **Eu^{3+}** ions.

(Ground term: ^7F_o or $^7F_1$)

Transition $\Psi_J \rightarrow \Psi_{J'}$	Energy (cm^{-1})	$\| U^2 \|^2$	$\| U^4 \|^2$	$\| U^6 \|^2$
$^5K_5$	1156	0.0693	0.0961	0.1168
$^5I_7$	1997	0.0012	0.0884	0.1098
$^5I_6$	2449	0.0132	0.1269	0.0125
$^5I_8$	2464	0.0000	0.0183	0.0752
$^5I_5$	3006	0.3470	0.1642	0.2492
$^5I_4$	3351	0.0001	0.1672	0.0796
$^5F_5$	3414	0.0028	0.007	0.0004
$^5F_4$	3921	0.0025	0.0481	0.0017
$^5F_1$	4074	0.0000	0.0000	0.0045
$^5F_3$	4343	0.0000	0.13	0.0001
$^5F_2$	4382	0.0000	0.4122	0.0007
$^3P_0$	4477	0.0000	0.0000	0.0033
$^5H_5$	5970	0.0006	0.0037	0.0126
$^5H_6$	5973	0.0306	0.143	0.0001
$^5H_4$	6201	0.077	0.0344	0.0037
$^5H_7$	6439	0.0001	0.0208	0.0925
$^5H_3$	6641	0.0000	0.1218	0.0916
$^5L_{10}$	9031	0.0000	0.0000	0.0064
$^5L_9$	9524	0.0000	0.0083	0.0181
$^5D_4$	9848	0.0001	0.0005	0.1279
$^5L_8$	10268	0.0011	0.0053	0.0104
$^5G_5$	10787	0.0001	0.0004	0.1695
$^5G_6$	10793	0.0148	0.0104	0.1116
$^5G_4$	10805	0.0001	0.0631	0.0056
$^5G_3$	10902	0.0000	0.1132	0.0506
$^5G_2$	11104	0.0000	0.0419	0.0034
$^5L_7$	11179	0.2634	0.0712	0.0848
$^5L_6$	12225	0.1065	0.0001	0.3866
$^5D_3$	13107	0.0000	0.0071	0.1140
$^5D_2$	15998	0.0000	0.0001	0.0225
$^5D_1$	18462	0.0000	0.0000	0.0042
$^5D_0$	20192	0.0000	0.0000	0.0142
$^7F_6$	32535	0.0000	0.0001	0.0084
$^7F_5$	33615	0.0001	0.0000	0.0041
$^7F_4$	34666	0.0001	0.0012	0.0002
$^7F_3$	35626	0.0000	0.0046	0.0031
$^7F_2$	36475	0.0000	0.0024	0.0006
$^7F_1$	37136	0.0000	0.0000	0.0004
$^7F_0$	37513	0.0000	0.0000	0.0009

Summing up the $A_{JJ'}$ quantities over all possible final states, one can get the radiative life time τ of an excited energy level as,

$$\tau = \frac{1}{\sum_{J'} A_{JJ'}} \tag{1.41}$$

Finally, the branching ratio $\beta_{JJ'}$ is evaluated using

$$\beta_{JJ'} = \frac{A_{JJ'}}{\sum_{J'} A_{JJ'}}. \tag{1.42}$$

This analysis on photoluminescence and optical absorption data, guide us to know to what extent the present glasses can be used as laser hosts.

1.3 Brief review of the previous work on TeO_2 based glasses

Surendra Babu *et al.* [64] have recently reported spectroscopic investigations of 1.06 μm emission in Nd^{3+}-doped alkali niobium zinc tellurite glasses. In this system the authors have observed that the quantum efficiency of the $^4F_{3/2}$ level is higher than the typical value of the other tellurite based glasses. Sandhya Rani *et al.* [65] have studied the electrical and magnetic properties of copper doped tellurite glass system. These studies have indicated the coexistence of antiferromagnetic (AFM) as well as ferromagnetic (FM) interactions between Cu^{2+} ions in these glasses. Yousef *et al.* [66] have reported thermal characteristics and crystallization kinetics of tellurite glass with small amount of additive As_2O_3. In this study the authors have reported crystallization results are analyzed, and both the activation energy of crystallization process and the crystallization mechanism were discussed in

detail. Upender *et al.* [67, 68] have reported the structure, physical and thermal properties of WO_3-TeO_2 glasses. In this study the variations in the optical band gap energy (E_{opt}) and optical basicity (Λ_{th}) with WO_3 content have been discussed in terms of the glass structure. Jlassi *et al.* [69] have studied photoluminescence quenching in Er^{3+}-doped tellurite glasses. In this study it was found that PL quenching with Er concentration in the tellurite glass is independent of OH- content. The authors have also determined stimulated cross-section at 1.53 μm and have discussed using the McCumber theory. Cherif *et al.* [70] have reported red fluorescence under 980 nm excitation in Er^{3+} doped TeO_2–ZnO glasses. The dynamics of the red up-conversion was well explained in this report. Starvou *et al.* [71] have investigated Raman scattering boson peak and differential scanning calorimetry studies of the glass transition in tellurium-zinc oxide glasses. The studies of these results have indicated that the Boson peak is highly sensitive to dynamical effects over the glass transition and provides a means for an equally reliable (to DSC) determination of T_g in tellurite glasses and other network glasses. Ardelean *et al.* [72] have reported Infrared and Raman spectroscopic studies of MnO–As_2O_3–TeO_2 glass system. In this study the authors have reported the presence of MnO_2 units in this glass network. Soulis *et al.* [73] have studied second harmonic generation induced by optical poling in TeO_2–Tl_2O–ZnO glasses. In this study the authors have concluded that the second order non-

linearity amplitude is increasing with increase of Tl_2O concentration in the glass network. Ozdanova *et al.* [74] reported optical band gap and Raman spectra some tellurite glass systems. In this study the authors have found that structural changes are induced by chemical composition in TeO_2 network due to conversion from TeO_4 trigonal bipyramids to TeO_3 and TeO_{3+1} units. Hayakawa *et al.* [75] have investigated the nonlinear optical properties and glass structure for $MO–Nb_2O_5–TeO_2$ (M = Zn, Mg, Ca, Sr, Ba) glasses. In this study the authors have measured the third-order nonlinear optical susceptibilities $\chi(3)$ of these glasses by Z–scan measurement using Ti:Sapphire femtosecond laser pulses. Wang *et al.* [76] have reported optical properties and supercontinuum generation of TeO_2-based glass. In this report the authors have studied thermal stability, optical transmittance, nonlinear optical properties and supercontinuum generation of TeO_2–based glass and demonstrated and it is a potential candidate in application in optical devices. Sidek *et al.* [77] have studied optical properties of ZnO-TeO_2 glass system. In this study the authors have found that the optical band gap (Eopt) of zinc tellurite glass decreases with increasing of ZnO content and attributed to the increment of Non-Bridging Oxygen (NBO) ion contents in the glass network. Dimitrov and Komastru [78] have reported changes of coordination number of tellurium and group optical basicity of ZnO-TeO_2 glasses. In this study it has been proposed that the optical basicity of $ZnO–TeO_2$ glasses decreases with increasing

modifier content due to the formation of TeO_3 groups in the structure which possess lower group optical basicity than that of TeO_4 groups. Ozdanova *et al.* [79] have reported optical band gap and Raman spectra of bismuth tungsten tellurite and lead tungsten tellurite glasses. In this study it was reported that tungsten ions participate in the glass network with WO_6 corner shared octahedral units and the linkages of the type Bi–O–Te, Pb–O–Te and W–O–Te are also possible in the glass network.

Sidkey *et al.* [80] have studied relaxation of longitudinal ultrasonic waves in binary TeO_2–Nb_2O_5 and ternary TeO_2–Nb_2O_5–LiO_2 tellurite glass systems in the temperature range 200-280 K. The results showed that the mean activation energy is dependent on the modifier content. Abd El-Moneim [81] has investigated DTA and IR absorption spectra of vanadium tellurite glasses and reported that the structure of the glass system changes at 20 mol% of V_2O_5. Silva *et al.* [82] have prepared TeO_2–PbO glasses and investigate the structure by means of Raman scattering and X–ray absorption spectroscopy. Lezal *et al.* [83] have studied physical properties of TeO_2–PbO–$PbCl_2$, TeO_2-ZnO and Ga_2O_3–PbO–Bi_2O_3 glasses. Vijaya Prakash *et al.* [84] have investigated physical and optical properties of niobium based tellurite glasses and concluded that the large refractive index values obtained are due to the hyperpolarisability of the Nb–O bands. Pal *et al.* [85] have prepared MoO_3–TeO_2 glasses by melt quenching and studied the d.c. conductivity.

Elkholy and Sharaf [86] studied the dielectric properties of TeO_2–P_2O_5 glasses and found the dielectric constant and loss decreased with increasing frequency and increased with increasing temperature. El-Damarawi *et al.* [87] have investigated ionic conductivity of mixed cationic glasses containing silver ions and observed that the values of conductivity in both phosphate and tellurite glasses are similar. Mori *et al.* [88] prepared V_2O_5-Sb-TeO_2 glasses by press quenching and studied the small polaron hopping conduction in the glasses. Iwadate *et al.* [89] investigated the short-range structure of K_2O–TeO_2 by XRD and semi-empirical molecular orbital calculation method and found that amorphous alkali tellurites consisted of TeO_4 trigonal bipyramids and TeO_3 trigonal pyramids. Murali and Rao [90] have carried out spectroscopic investigations on Cu (II) ions doped in alkali lead boro tellurite glasses and observed that optical energy gap decreased and Urbach energy increased with increase in concentration of copper ion.

Kosuge *et al.* [91] have reported that the K_2O–WO_3–TeO_2 glasses with 60-70 mol % of TeO_2 are thermally stable against crystallization. Chowdari and Kumari [92] studied the structure and ionic conduction in the Ag_2O-WO_3-TeO_2 glass system. The results showed that the glass network consists of TeO_4, TeO_3, WO_4 and WO_6 polyhedra. Ravikumar *et al.* [93] have investigated the dielectric properties of CuO doped ZnF_2–PbO–TeO_2 glasses and concluded that the dielectric parameters are strongly dependent on the concentration of

CuO. Their infrared spectral investigations [94] on these glasses showed that an increase in the concentration of PbO leads to an increase in the degree of depolymerisation of the glass network. Turrell *et al.* [95] have investigated the effect of doping metal on the structure of binary tellurium oxide glasses by Raman spectroscopy and found that the positions of Raman bands depend both on the metal oxide and the amount of doping. Pan and Morgan [96] have studied the Raman spectra and thermal analysis of lead tellurium germanate glasses and observed that the glass transition temperature decreased with increase in TeO_2 content up to 40 mol%. Shaltout *et al.* [97] have studied the optical properties of TeO_2-WO_3 glass system by Fourier transform infrared spectroscopy in the spectral range 150–25,000 cm^{-1} and reported that the optical band gap decreased while the refractive index increased with increase in WO_3 content. Sakata *et al.* [98] have studied the dc conductivity of V_2O_5–PbO–TeO_2 glasses and explained it on the basis of small polaron hopping theory. Ravikumar and Veeraiah [99] carried out a considerable work on various physical properties of ZnF_2-PbO-TeO_2 glass system doped with certain rare earth ions. They studied the optical absorption and photoluminescence properties of Eu^{3+} doped ZnF_2–PbO–TeO_2 glasses.

Mazzuca *et al.* [100] have undertaken structural studies of ZnO-TeO_2 glass system by Raman scattering and interpreted the sharp bands in the final spectra on the basis of chains of TeO_3–TeO_4 polyhedra interlaced with chains

of ZnO_6 groups. Sekiya *et al.* [101] have investigated the MoO_3-TeO_2 glasses by Raman spectrsopy and differential thermal analysis and reported that the glasses contain TeO_4 trigonal bipyramids, TeO_{3+1} polyhedra and MoO_6 octahedra as basic structural units. Balaya and Sunanda [102] have investigated the mixed alkali effect, in the conductivity of TeO_2 glasses. They have discussed their results in the light of intercharge transportation phenomenon. Mallawany [103] gave a detailed theoretical analysis of electrical properties of tellurite glasses containing some transition metal ions and concluded that the conduction in these glasses is mainly due to hopping of small radius polarons. Mori *et al.* [104] have reported the electrical conductivity of V_2O_5–Sb_2O_3–TeO_2 glasses. They have found that these glasses are of n-type semiconductors. Mallawany [105] has studied the longitudinal elastic constants of ZnO–TeO_2 glass system. His results have indicated that the longitudinal elastic constants are strongly dependent on the composition of the glasses. Also Mallawany with Sidkey *et al.* [106] has measured the ultrasonic velocity in MoO_3-TeO_2 glass system using pulse echo technique and they have used this data to determine the elastic moduli, Debye temperature and Poisson's ratio of the glasses. Satyanarayana and Buddhudu [107] have measured the elastic properties of Nd^{3+} doped TeO_2–V_2O_5, GeO_2–V_2O_5–TeO_2 and TeO_2–V_2O_5–R_2O (R_2O is alkali oxide) glasses by the ultrasonic technique. Dimitrov *et al.* [108] have investigated the effect of WO_3 on IR spectra of

tellurite glasses. Ahmed [109] has reported the optical absorption spectrum of tellurium in alkali borate glasses. Bhagat *et al.* [110] have reported d.c. conduction phenomenon along with some other physical properties of TeO_2–Fe_2O_3 glasses doped with certain rare earths. They found that the activation energy and dc conductivity are the function of atomic number Z of the rare earth cations. Wang *et al.* [111] have studied the infrared properties of TeO_2–PbO–$PbCl_2$ glass system and assigned the various bands obtained due to TeO_3 and TeO_4 units.

1.4 Motivation and objective of the present work

TeO_2 based glasses like ZnF_2–As_2O_3–TeO_2, have attracted an enhanced interest in recent years. Tellurite glasses are well known due to their high dielectric constant, high refractive index, large third order non-linear susceptibility, good chemical resistance and good infrared transmissivity. Furthermore, these glasses are transparent from ultraviolet to the middle infrared region. They are resistant to atmospheric moisture and are capable of accepting large concentrations of transitional metal ions and rare-earth ions. Further, the inclusion of interesting transition metal ions (vanadium and nickel) into the tellurite glass network is an added advantage to use these materials for solid state ionic devices and for broad band optical amplifiers. The studies on dielectric properties over a range of frequency and temperature of these glasses helps in assessing their insulating character but also throw light on structural

aspects of these glasses when these studies are coupled with data on spectroscopic properties.

Further, the WO_3 mixed tellurite glasses offer suitable environment for rare earth ions to exhibit high luminescence efficiencies. In view of this, fluorescence characteristics of three interesting rare earth ions (Nd^{3+}, Sm^{3+} and Eu^{3+}) that exhibit high luminescence efficiencies in visible and NIR regions in these glasses have also been investigated.

Thus the clear objectives of the present study are to prepare, characterize and

- To have a comprehensive understanding over the influence of **vanadium** ions on structural aspects of ZnF_2–As_2O_3–TeO_2 glasses by investigating the dielectric properties, optical absorption, ESR, IR and photoluminescence.
- To have a broad perceptive over the role of **nickel** ions on the structure of ZnF_2–As_2O_3–TeO_2 glass system from a systematic study of various dielectric properties coupled with spectroscopic and magnetic studies.
- To investigate the luminescence efficiencies of three rare earth ions (viz., Nd^{3+}, Sm^{3+} and Eu^{3+}) in ZnF_2–WO_3–TeO_2 glasses and to examine the possible uses of these glasses laser hosts.

1.5 Contents of the present work

The glasses used for the present studies are:

4. V_2O_5 series: $20ZnF_2–30As_2O_3–(50–x)\ TeO_2$: x V_2O_5 $(0 \le x \le 0.6)$
5. NiO series: $20ZnF_2–30As_2O_3–(50–x)TeO_2$: xNiO $(0 \le x \le 2.0)$
6. Ln_2O_3 series: $(50–x)ZnF_2–xWO_3–49TeO_2$: $1Ln_2O_3$ $(5 \le x \le 20)$

   (where Ln = Nd, Sm and Eu)

The studies carried out are:

(vii) differential scanning calorimetry and the evaluation of glass transition temperature T_g;

(viii) infrared spectral studies in the wavenumber range 400–2000 cm^{-1} and the study of the effect of concentration of transition metal ions on the position and intensity of various vibrational bands;

(ix) optical absorption studies in the wavelength range 300–2100 nm, identification of various electronic transitions of transition metal ions;

(x) electron spin resonance measurements and the identification of the positions and valence states of titanium ions in the glass network;

(xi) dielectric properties viz., dielectric constant ε^{l}, dielectric loss tan δ and ac conductivity σ_{ac} in the frequency range $10^2–10^5$ Hz and in the temperature range 30–250 ^oC;

(xii) optical absorption, fluorescence studies of Nd^{3+}, Sm^{3+} and Eu^{3+} ions doped $ZnF_2–WO_3–TeO_2$ glasses.

References

[1] W.H. Zachariasen, *J. Am. Chem. Soc.*54 (1932) 3841.

[2] W. Vogel, *Glass Chemistry* (Springer Verlag, Berlin 1994)

[3] S.R. Elliott, *Physics of Amorphous Materials* (Longmann, Essex, 1990).

[4] D.E. Polk, *Scripta metall.* 4 (1970) 117.

[5] K.J. Rao, *Structural Chemistry of Glasses,* (Elsevier, Amasterdam, 2002).

[6] M.D. Ingram, *Phys. Chem. Glasses* 28 (1987) 215.

[7] James E Shelby, *Introduction to Science and Technology of Glass Materials* (Royal Society of Chemistry, 2005).

[8] N. Vedeanu, O. Cozar, I. Ardelean, B. Lendl, D.A. Magdas, *Vibr. Spectr.* 48 (2008) 259.

[9] S. Daoudi, L. Bejjit, M. Haddad, M.E. Archidi, A. Chahine, M. Et-tabirou, P. Molinié, *Spectro. Lett*. 40 (2007) 785.

[10] G. Murali Krishna, Y. Gandhi and N. Veeraiah, *Phys. Stat. Solidi (a)* 205 (2008) 177.

[11] G. Srinivasa Rao and N. Veeraiah, *J. Solid State Chem*.166 (2002) 104.

[12] X. Li, X. Wang, D. He, J. Shi, *Mater. Chem*. 18 (2008) 4103.

[13] Z.A. Talib, W.M. Daud, E.Z.M. Tarmizi, H.A.A. Sidek, W.M.M. Yunus, *J. Phys. Chem. Solids* 69 (2008) 1969.

[14] J.E. Stanworth, *J. Soc. Glass Technol.* 36 (1952) 217.

[15] J.E. Stanworth, *J. Soc. Glass Technol.* 36 (1954) 425.

[16] J.E. Stanworth, *Nature* 169 (1952) 581.

[17] J.S. Wang, E.M. Vogel, E. Snitzer, *Opt. Mater.* 3 (1994) 187.

[18] H. Burger, W. Vogel and V. Kozhukharov, *Infrared Phys.* 25 (1985) 395.

[19] G. Ozen, J.P. Denis, M.Genotelle and F. Pelle, *J. Phys. Cond. Matter* 7 (1995) 4325.

[20] H.Oishi, Y. Benino and T. Komatsu, *Phys. Chem. Glasses* 40 (1999) 212.

[21] J. Wang, L. Reekie, W.S. Brocklesby, Y.T. Chow and D.N. Payne, *J. Non-Cryst. Solids* 180 (1997) 207.

[22] S. Neov, V. Kozhukharov, I. Gerasimova, K. Krezhov and B. Sidzhimov, *J. Phys. C* 12 (1979) 2475.

[23] B.V. Raghavaiah, N. Veeraiah, *J. Phys. Chem. Solids* 65 (2004) 1153.

[24] K. Nassau, *Bell Syst. Tech. J.* 60 (1981) 327.

[25] A. Bishay, C. Maghrabi, *Phys. Chem. Glasses* 10 (1969) 1.

[26] M.M. El-Desoky, S.M. Abo-Naf, *J. Mater. Sci.* 15 (2004) 425.

[27] J.C. Sabadel, P. Armand and P. Baldeck, *J. Sol. Stat.Chem.*132 (1997) 411.

[28] C.V. Reddy, N.Y. Ahmed, R.R. Reddy and T.V.R. Rao, *J. Phys. Chem. Solids* 159 (1998) 337.

[29] G. El-Damrawi, S. Abd-El-Maksoud, *Phys. Chem. Glasses* 41 (2000) 6.

[30] R.N. Hampton,Wan Hong, G.A. Saunders, *J. Non-CrystSolids* 94 (1987) 307.

[31] G.D.L.K. Jayasinghe, D. Coppo and P.W.S.K. Bandaranayake, *Solid State Ion. Diffus. React.* 76 (1995) 297.

[32] M. M. El-Samanoudy, *J. Mater. Sci.* 30 (1995) 3919.

[33] S. Inque, A. Nukui and K. Yamamoto, *Appl. Opt.* 37 (1998) 48.

[34] W.T. Carnall, P.R. Fields, K. Rajn, *J. Chem. Phys.* 49 (1968) 4424.

[35] F. Auzel, *Spectroscopy of Solid State Lasers* [B. Bibartaro, ed.] (Plenum, New York 1987).

[36] G. Guery J.L. Adam, *J. Lumin.* 42 (1988) 132.

[37] M.J. Weber and R. Cropp, *J. Non- Cryst. Solids* 4 (1981) 137.

[38] P. Butcher, K.J. Hyden, *Phil. Mag.* 36 (1997) 657.

[39] B. Tareev, *Physics of Dielectric Materials, (Mir, Moscow*, 1979).

[40] B.N. Figgis, M.A. Hitchman, Ligand *Field Theory and its Applications* (Wiley-VCH Verlag GmbH, Berlin, 2000).

[41] A. West, A.R. West, *Solid State Chemistry and Its Applications,* (John Wiley & Sons, Berlin, 1991).

[42] J.D. Lee, *Concise Inorganic Chemistry*, (Blackwell Science, London, 1999).

[43] Y. Tanabe and S. Sugano, *J. Phys. Soc. Japan* 9 (1954) 753.

[44] J.S. Griffith, *The Theory of Transition Metal Ions (*Cambridge University Press, London, 1964).

[45] R.A. Smith, *Wave Mech. Crystalline Solids (*Chapman and Hall, London, 1969).

[46] M. Bersohn and J.C. Baird, *An introduction to Electron Paramagnetic Resonance (*Benjamin Inc, New York 1966).

[47] A. Abragam and B. Bleaney, *Electron Paramagnetic Resonance of Transition Ions*, (Claredon Press, Oxford, 1970).

[48] C.P. Poole, Electron Spin Resonance: *A Comprehensive Treatise on Experimental Techniques*, (John Wiley, New York 1984).

[49] J.R. Pilbrow, *Transition Ion Electron Paramagnetic Resonance*, (Claredon Press, Oxford, 1990).

[50] J.A. Weil, J.R. Bolton, J.E. Wertz, *Electron Paramagnetic Resonance Elementary Theory and Practical Applications*, (John Wiley, New York 1994).

[51] M.H.L. Pryce, *Proc. Phys. Soc. A* 63 (1950) 25.

[52] A. Abragam, M.H.L. Pryce, *Proc. Roy. Soc. A* 205 (1951)135.

[53] R.J. Elliot, K.W.H. Stevens, *Proc. Roy. Soc. A* 218 (1953) 553.

[54] P.B. Ayscough, *Electron Spin Resonance in Chemistry*, (Methuen, London, 1967).

[55] P. Tarte, *Spectrochim. Acta* 18 (1962) 467.

[56] P. Tarte, *Physics of Non-Crystalline Solids* (Elsevier, Amsterdam, 1964).

[57] J.C. Sabadel, P.Armand, D. Cachau-Herreillat, P. Baldeck, O. Doclot, A. Ibanez and E. Philippot, *Solid State Chem*. 132 (1997) 411.

[58] S. Hufner, *Optical Spectra of Transparent Rare Earth Compounds*, (Plenum, New York 1968).

[59] B.R. Judd, *Phys. Rev*. 127 (1962) 750.

[60] G.S. Ofelt, *J. Chem. Phys*., 37 (1962) 511

[61] G. Guery, J.L. Adam, *J. Lumin*. 42 (1988) 132.

[62] M.J. Weber, R. Cropp, *J. Non-Cryst. Solids* 4 (1981) 137.

[63] M.J. Weber, *J. Chem. Phys*. 48 (1968) 4774.

[64] S. Surendra Babu, R. Rajeswari, K. Jang, C. Eun Jin, K. Hyuk Jang, H. Jin Seo, C.K. Jayasankar, *J. Lumin.* 130 (2010) 1021

[65] P. Sandhya Rani, R. Singh, *J. Mater. Sci.* 45 (2010) 2868

[66] E. Yousef, A. El-Adawy, M.H. Makled, A.E. Al-Salami, *J. Mater. Sci.* 45 (2010) 2930

[67] G. Upender, C.P. Vardhani, S. Suresh, A.M. Awasthi, V. Chandra Mouli, *Mater. Chem. Phys.* 121 (2010) 335

[68] G. Upender, V.G. Sathe, V.C. Mouli, *Physica B* 405 (2010) 1269

[69] I. Jlassi, H. Elhouichet, M. Ferid, R. Chtourou, M. Oueslati, *Opt. Mater.* 32 (2010) 743

[70] A. Cherif, A. Kanoun, N. Jaba, *Opt. Appl.* 40 (2010) 109

[71] E. Stavrou, C. Tsiantos, R.D. Tsopouridou, S. Kripotou, A.G. Kontos, C. Raptis, B. Capoen, (...), S. Khatir, *J. Phys. Cond. Matt.* 22 (2010) 195103

[72] I. Ardelean, S. Lupsor, D. Rusu, *Physica B* 405 (2010) 2259

[73] M. Soulis, J.R. Duclère, T. Hayakawa, V. Couderc, M. Dutreilh-Colas, P. Thomas, *Mater. Res. Bull.* 45 (2010) 551

[74] J. Ozdanova, H. Ticha, L.Tichy, *J. Optoelect. Adv. Mater.* 12 (2010) 1024

[75] T. Hayakawa, M. Hayakawa, M. Nogami, P. Thomas, *Opt. Mater.* 32 (2010) 448

[76] G. Wang, H. Fan, K. Li, G. Gao, L.Hu, *Pacific Rim Conference on Lasers and Electro-Optics, CLEO - Technical Digest*, 2009 art. no. 5292463

[77] H.A.A. Sidek, S. Rosmawati, Z.A. Talib, M.K. Halimah, W.M. Daud, *Am. J. Appl. Sci.* 6 (2009) 1489

[78] V. Dimitrov, T. Komatsu, *Phys. Chem. Glasses* 50 (2009) 395

[79] J. Ozdanova, H. Ticha, L.Tichy, *J. Non-Cryst. Sol.* 355 (2009) 2318.

[80] M.A. Sidkey, R.A. El-Mallawany, A.A. Abousehly and Y.B. Saddeek, *Mat. Chem. Phys.* 74 (2002) 222.

[81] A. Abd El-Moneim, *Mat. Chem. Phys*. 73 (2002) 518.

[82] M.A.P. Silva, Y. Messaddek, S.J.L. Ribeiro, M. Poulain and F. Villain, *J. Phys, Chem. Solids*, 62 (2001) 1055.

[83] D. Lezal, J. Pedlikova, P. Kostka, J. Bludska, M. Poulain and J. Zavadil, *J. Non-Cryst. Solids*, 284 (2001) 288.

[84] G. Vijaya Prakash, D. Narayana Rao and A.K. Bhatnagar, *Solid State Comm.* 119 (2001) 39.

[85] M. Pal, K. Hirota, Y. Tsuji gami, H. Sakata *J. Phys. D* 34 (2001) 459.

[86] 109. M.M. Elkoholy and L.M. El-Deen Sharaf, *Mat. Chem. Phys.* 65 (2000) 192.

[87] G. El-Damarawi, A.K. Hassan and H. Doweidar, *Physica B*, 29 (2000) 34.

[88] H. Mori, H. Matsuno and H. Sakata, *J. Non-Cryst. Solids,* 276 (2000) 78.

[89] Y. Iwadate, T. Mori, T. Hattori *et al. J. Alloys Comp*. 311 (2000) 153.

[90] A. Murali and J.L. Rao, *J. Phys. Cond. Mat*. 11 (1999) 7921.

[91] T. Kosuge, Y. Benino, V. Dimitrov, R. Sato and T. Komatsu, *J. Non-Cryst. Solids*, 242 (1998) 154.

[92] B.V.R. Chowdari and P.P. Kumari, *J. Mat. Sci.* 33 (1998) 3591.

[93] V. Ravi Kumar, N. Veeraiah, S. Buddhudu and V, Jaya Tyaga Raju, *J. Phys. III France,* 7 (1997) 951.

[94] V. Ravi Kumar and N. Veeraiah, *J. Mater. Sci. Lett*. 16 (1997) 1816.

[95] S. Turrell, C. Duverger and M. Bouazaui, *J. Non-Cryst. Solids*, 220 (1997) 169.

[96] Z. Pan and S.H. organ, *J. Non-Cryst. Solids*, 210 (1997) 130.

[97] I. Shaltout, Y. Tang, R. Braunstein and E.E. Shaisha, *J. Phys. Chem. Solids,* 57 (1996) 1223.

[98] H. Sakata, M. Amano and T. Yagi, *J. Non-Cryst. Solids*, 194 (1996) 198.

[99] V. Ravi Kumar and N. Veeraiah, J. Mater. Sci. 33 (1998) 2659; *Phys. Stat. Solidi (a)*, 147 (1995) 601.

[100] M. Mazzuca, J. Portier, B. Tanguy, F. Romain and S. Turrell, *J. Molecular Struc.* 349 (1995) 413.

[101] T. Sekia, N. Mochida and S. Ogawa, *J. Non-Cryst. Solids,* 185 (1995) 135.

[102] P. Balaya and C.S. Sunandhana, *J. Non. Cryst. Solids* 175 (1994) 51.

[103] R. EL- Mallawany, *Mater. Chem. Phys.* (Switzerland) 37 (1994) 224.

[104] H. Mori, T. Kitami and H. Sakata, *J. Non-Cryst. Solids.* 168 (1994) 157.

[105] R. EL- Mallawany, *J. Appl. Phys.* 73 (1993).

[106] R. EL- Mallawany, M. Sidkey, S. Khafasy and H. Afifi, *Mater. Chem. Phys.* 37 (1994) 295.

[107] J.V. Satyanarayana, S. Bhuddudu, *J. Alloys Compd.* 214 (1994) 97.

[108] M. Dimitrova-Pankova, Y. Dimitriev, M. Aranaudov and V. Dimitrov, *Phy. Chem. Glasses,* 30 (1989) 260.

[109] A.A. Ahmed, *J. Non-Cryst. Solids,* 70 (1989) 17.

[110] M.N. Khan, M. A. Hassan and C.A. Hogarth, *Phys. Stat. Sol. (a),* 104 (1988) 181.

[111] Yu- Hu Wang, A. Osaka, Y. Miura, J. Takada, K. Oda and K. Takahashi, *Mat. Sci. Forum,* 32 (1988) 161.